IOP PUBLISHING JOURNAL OF PHYSICS D: APPLIED PHYSICS

J. Phys. D: Appl. Phys. **42** (2009) 163001 (18pp) doi:10.1088/0022-3727/42/16/163001

TOPICAL REVIEW

Plasmas for spacecraft propulsion

C Charles

Space Plasma, Power and Propulsion Group, Research School of Physics and Engineering,
The Australian National University, ACT 0200, Australia

E-mail: christine.charles@anu.edu.au

Received 14 April 2009
Published 31 July 2009
Online at stacks.iop.org/JPhysD/42/163001

Abstract

This review presents the basics of plasma discharges applied to electric spacecraft propulsion. It briefly reports on the mature and flown technologies of gridded ion thrusters and Hall thrusters before exploring the recent yet immature technology of plasma thrusters based on expansion from low pressure high density inductively coupled and wave-excited plasma sources, e.g. the radiofrequency helicon source. Prototype development of plasma engines for future space travel is discussed using the example of the helicon double layer thruster. A summary of highlights in electric propulsion based space missions gives some insight into the challenges of future high power missions in more remote regions of space.

(Some figures in this article are in colour only in the electronic version)

1. Introduction

Several hundred electric thrusters are currently operating on commercial communications satellites. A few examples of successful deep-space scientific missions with ion gridded thrusters (DEEP-SPACE 1 mission to Comet Borelly) and Hall thrusters (SMART 1 mission to the Moon) operating as primary propulsion engines have generated increasing interest in the further development of electric propulsion for future high power missions (Jahn and Choueiri 2002, Martinez-Sanchez and Pollard 1998, Brophy and Noca 1998, Frisbee 2003 and Choueiri 2004). This review aims to discuss plasma discharges applied to the field of spacecraft propulsion. It is not comprehensive and many propulsion systems are not reported for lack of space. Thrusters basics, types and applications in space are given in section 2.

Recent reviews (Zhurin *et al* 1999) and textbooks (Goebel and Katz 2008) on the well-established and successfully flown Hall thrusters and ion gridded thrusters provide detailed information on the 'ion engine' fundamentals and their optimization for electric propulsion applications. Here, the main focus is to present the early days of electrode-less magneto-plasma thrusters research and development for future missions with 'plasma' engines. These were already described in 1968 by Jahn (Jahn 2006). The aim is not to compare thruster performance between established technology and immature technology but to draw upon four decades of knowledge on 'ion' engines and four decades of knowledge on the development of plasma sources for the microelectronics industry to present the main aspects and limitations inherently associated with the development of 'plasma' engines.

Section 3 presents the basics of plasma discharges applied to propulsion. Here electrode-less magnetoplasma thrusters are defined as low pressure high density inductively coupled or wave-excited plasmas expanding and accelerating into space without the use of electrostatically biased grids in the exhaust. Section 4 briefly describes these plasma sources and uses the example of the radiofrequency helicon source. The relationship between plasma parameters and resulting thrust is discussed. Section 5 presents the helicon double layer thruster (HDLT), based on a magnetized plasma expansion with an electrostatic shock and discusses the complexity and challenges, but also new parameter control of future 'plasma' engines. Finally, section 6 presents highlights of successful ion engine based space missions and discusses the future of magnetized plasma engines for high power deep-space missions.

Sections 2, 3 and 4 in this review are largely based on the books by Goebel and Katz (2008), Jahn (2006) and Lieberman and Lichtenberg (1994). Sections 5 and 6 often refer to previous work on the helicon source and on the HDLT, by the

[1] Author to whom any correspondence should be addressed.

space plasma, power and propulsion group at the Australian National University (ANU), which are essentially used as examples to derive the main parameter range of 'plasma' engines.

2. Thruster basics

2.1. Main parameters

The thrust or force provided to a spacecraft results from the ejection of propellant from the engine exhaust into space. The thrust is the time rate of change of the momemtum of the propellant:

$$T = \frac{\mathrm{d}(m_\mathrm{p} v_\mathrm{ex})}{\mathrm{d}t} = v_\mathrm{ex}\frac{\mathrm{d}(m_\mathrm{p})}{\mathrm{d}t}, \tag{1}$$

where m_p is the propellant mass and v_ex is the propellant exhaust velocity (assumed constant). T is expressed in newtons, v_ex in km s^{-1} and $\frac{\mathrm{d}(m_\mathrm{p})}{\mathrm{d}t}$ in kg s^{-1}. In laboratory experiments, a common unit of gas flow is sccm (standard cubic centimetre per minute), e.g. 1 sccm of argon and xenon corresponds to 0.03 mg s^{-1} and 0.098 mg s^{-1}, respectively.

In chemical propulsion, the thrust results from the combustion of propellant in a chamber which then expands in a nozzle. The exhaust velocity of the ejected neutral particles depends on the propellant molecular and chemical properties (e.g. hydrazine N_2H_4) and on the engine expansion ratio (Turner 2009). Although v_ex is limited to about 3–5 km s^{-1}, large thrust (up to meganewtons) can be achieved.

In electric propulsion, the thrust results from ejecting charged particles. An electric power source is used to create and accelerate the charge particles. Since charged particles 'react' to electric and magnetic fields, higher exhaust velocities can be achieved, typically in the range 5–50 km s^{-1}. The thrust is orders of magnitude lower than that of chemical rockets as the propellant input is limited by the discharge characteristics: a chemical propellant input of 1 g s^{-1} generates a thrust of a few newtons in a chemical thruster while a xenon input of 1 mg s^{-1} will generate a thrust of a few tens of millinewtons in an electric thruster. Low thrust results in longer missions.

The specific impulse, or ratio between the thrust and the rate of propellant consumption by sea-level weight, can be expressed as the exhaust velocity divided by the gravitational acceleration, g (9.81 m s^{-2}):

$$I_\mathrm{sp} = \frac{T}{\frac{\mathrm{d}m_\mathrm{p}}{\mathrm{d}t}g} = \frac{v_\mathrm{ex}}{g}. \tag{2}$$

The I_sp is expressed in units of seconds and can be viewed as a measure of the propellant fuel consumption rate. High exhaust velocities or high I_sp allows maximization of missions payload mass and makes electric propulsion attractive. Other advantages of electric propulsion include the use of geodesic trajectories for deep-space missions and the ability to vary the I_sp throughout a mission, although it should be noted that the specific impulse will be effectively reduced by propellant not converted into charged particles.

The thrust, T_n, from any non-ionized propellant, can be estimated from the 'random' flux across a surface area, A (Braithwaite 2000), for an isotropic thermal distribution of temperature T_n (typically 300 K in argon and 500 K in xenon), which is

$$\Gamma_\mathrm{n} = \frac{1}{4} n_\mathrm{n} v_\mathrm{n} A, \tag{3}$$

where n_n is the neutral gas density, $v_\mathrm{n} = \sqrt{\frac{8kT_\mathrm{n}}{\pi M_\mathrm{m}}}$ and is the average velocity of the neutrals (M_n is the mass of the atom and k is the Boltzmann constant). Therefore

$$T_\mathrm{n} = v_{n_\mathrm{ex}}\frac{\mathrm{d}(m_\mathrm{m})}{\mathrm{d}t} = \frac{1}{4} n_\mathrm{n} v_\mathrm{n}^2 M_\mathrm{m} A, \tag{4}$$

where $v_{n_\mathrm{ex}} = v_\mathrm{n}$ is the exhaust velocity of the neutrals.

In electric propulsion, the charged particles are usually produced in a plasma and the main source of thrust results from the positively charged ions. From equation (1), the thrust from these ions is written as

$$T_\mathrm{i} = v_{\mathrm{i}_\mathrm{ex}}\frac{\mathrm{d}(m_\mathrm{i})}{\mathrm{d}t}, \tag{5}$$

where m_i is the ionized propellant mass and $v_{\mathrm{i}_\mathrm{ex}}$ is the ion exhaust velocity. If an ion is accelerated by a net voltage, V, then, by conservation of energy, its resulting velocity is

$$v_\mathrm{i} = \sqrt{\frac{2qV}{M_\mathrm{i}}}, \tag{6}$$

where q is the ion charge and M_i is the mass of the ion. Hence from equations (5) and (6), the thrust $T_{\mathrm{i}_\mathrm{b}}$ produced by a zero-divergence monoenergetic ion beam accelerated by a potential V_b before ejection will be

$$T_{\mathrm{i}_\mathrm{b}} = v_\mathrm{i}\frac{M_\mathrm{i} I_\mathrm{b}}{q} = \sqrt{\frac{2M_\mathrm{i}}{q}} I_\mathrm{b}\sqrt{V_\mathrm{b}}, \tag{7}$$

where I_b is the ion beam current. The thrust is proportional to the beam current, the square root of the ion mass and acceleration potential and inversely proportional to the square root of the ion charge. Various thruster designs and concepts to produce and eject an accelerated ion beam are discussed in the next sections. For space mission design, the performance of a prototype of exhaust diameter, D, is defined by its thrust for an input power and an input propellant rate (Goebel and Katz 2008).

2.2. Chemical thrusters

Equations (1) and (2) can be applied to chemical propulsion and the main chemical thrusters can be classified in the order of increased specific impulse (Turner 2009): thrusters based on a cold gas (e.g. nitrogen) expansion in a convergent–divergent nozzle, single use thrusters based on the combustion of a solid fuel 'block' and thrusters based on the expansion of hot reactants. In the latter, the chemical decomposition or combustion of a liquid fuel (single or bi-propellant system) produces 'hot reactants' which are expanded in a nozzle to maximize thrust. The fuel injection system and the combustion initiation scheme vary. For example, hydrazine (N_2H_4) is usually injected by capillarity into a chamber containing a

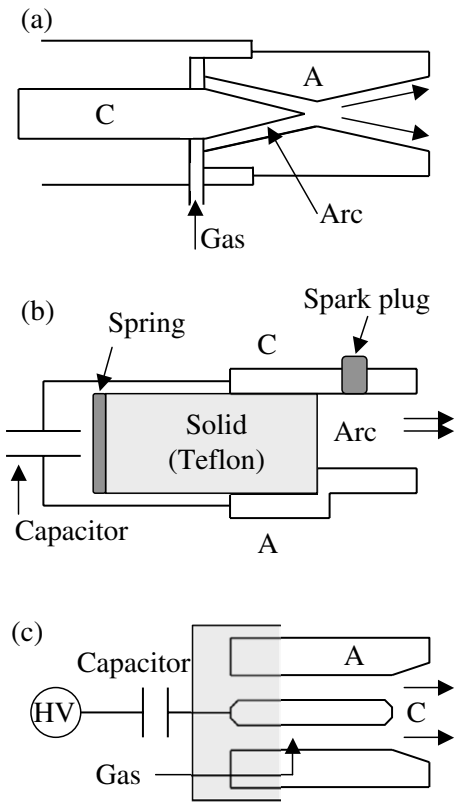

Figure 1. Schematic of the main 'arc-based' thrusters: (*a*) Arcjet thruster, (*b*) PPT and (*c*) MPD thruster; A = anode, C = cathode, HV = high voltage.

porous catalyst and the hot reactants are NH_3, N_2 and H_2. These are efficient, simple and reliable thrusters which produce high thrust, though over a finite duration. Trajectories are usually ballistic and there is virtually no control of I_{sp}. The main control parameter is the flowrate of injected propellant.

2.3. Electric thrusters

The primary motivation for the development of electric thrusters is the increase in I_{sp} (utilization of propellant mass). They are often classified in three categories based on the main heating mechanism (Jahn 2006, Turner 2009, Goebel and Katz 2008): electrothermal, electromagnetic and electrostatic thrusters.

To heat the propellant 'electrothermal' thrusters use either resistors ('Resistojet') or an electric arc ('Arcjet'). In the latter, a plasma in the form of a high current arc is created in a small volume encapsulated between a cathode and an anode as shown in figure 1(*a*) (Jahn 2006, Martinez-Sanchez and Pollard 1998, Frisbee 2003). The energy transfer from the arc ions to the neutrals is complex. In addition to the hot neutral propellant, the exhaust stream also contains ions, electrons and often sputtered cathode material.

Plasma arcs are also used in 'electromagnetic' thrusters such as the 'pulsed plasma thruster' (PPT) (Keidar *et al* 2000, Martinez-Sanchez and Pollard 1998, Jahn and Choueiri 2002, Frisbee 2003) and the 'magnetoplasmadynamic' (MPD) thruster, which is also called the 'Lorentz force accelerator' (LFA) (Jahn 2006, Martinez-Sanchez and Pollard 1998, Jahn and Choueiri 2002). In the PPT, a bar of solid propellant such as teflon is pushed by a spring in between a cathode and an anode and ablated, then ionized in a plasma arc (about 20 kA for a few microseconds). The ionized material is accelerated subsequently by the Lorentz force in the exhaust (figure 1(*b*)). PPTs have a very low thrust efficiency but high exhaust velocity (a few tens of km s^{-1}) and have been successfully flown, for example aboard the Soviet probes Zond 2 in 1964 or more recently the NASA Goddard SpaceFlight Center EO-1 spacecraft in 2000.

In an MPD thruster (Martinez-Sanchez and Pollard 1998, Tanabe 1994, Frisbee 2003), the propellant (inert gas, hydrazine or lithium) is ionized in a very high current arc generated between a central heated cathode and a surrounding anode (figure 1(*c*)) and accelerated by the Lorentz force (self-generated and in some cases with an additional applied magnetic field). Arc-based thrusters are summarized in figure 1 and will not be described further in this study.

The third class of thruster is based on 'electrostatic' heating (figure 2) and includes the field emission electrostatic propulsion (FEEP) thruster or 'colloid' thruster, the gridded ion thruster and the Hall thruster. The low power FEEP thruster (figure 2(*a*)) provides precision control of thrust (on the order of a micronewton or less) from single ions or electrically charged droplets extracted by field emission from small needles with a sharp tip filled with liquid metals (e.g. indium, caesium) and has been succesfully flown (Turner 2009, Martinez-Sanchez and Pollard 1998, Jahn and Choueiri 2002). In gridded ion thrusters (figures 2(*b*)–(*d*)) and Hall thrusters (figure 2(*e*)), the propellant is ionized in a plasma cavity and the positive ions are accelerated by an applied electrostatic field (Goebel and Katz 2008). These will be briefly reviewed and used as 'reference' cases in this study of 'electrode-less plasma' thrusters which are summarized in figure 3 and will be described in detail in the next sections.

2.4. Space applications

Due to their low thrust range (0.1 to about 100 mN) and vacuum requirement, electric thrusters can only be deployed in space. They can be used as a primary or secondary propulsion engine and applications include satellite station-keeping and deep-space exploration. Requirements vary depending on the type of manoeuvres to be executed: orbit raising or insertion, orbit control (North–South and East–West attitude control) or de-orbiting at the end of a satellite's lifetime. For future missions such as deep-space exploration, the power requirement for a fixed payload mass simply scales with the distance: typically 200 kW for a return mission to the outer solar system, 200–600 kW for a cargo tug to Mars and over 1 MW for a manned mission to Mars. This power cannot be achieved by solar-electric conversion only. Typically the path for a new spacecraft thruster from initial concept and research to commercialization and a space mission is costly and includes experimental and modelling studies in a laboratory, prototype design and fabrication, prototype tests on a thrust balance in a space simulation chamber, long duration lifetime testing, tests in a launch simulator, mission design and spacecraft integration, launch and deployment in space.

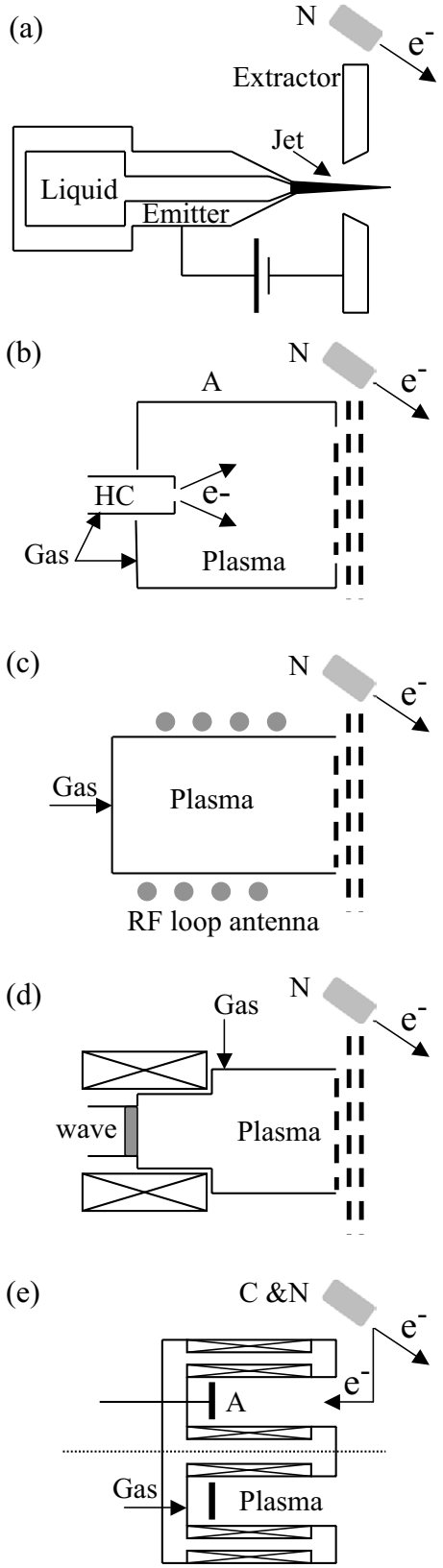

Figure 2. Schematic of the main 'electrostatic' thrusters: (*a*) field emission electrostatic propulsion (FEEP) thruster, (*b*) dc electron bombardment ion thruster, (*c*) RF ion thruster, (*d*) microwave ion thruster and (*e*) Hall thruster; A = anode, C = cathode, HC = hollow cathode, N = neutralizer; (*b*)–(*d*) are gridded ion thrusters with various excitation frequencies; (*b*) and (*c*) may be operated with solenoids or permanent magnets, e.g. Kaufman dc ion thruster (Goebel and Katz 2008).

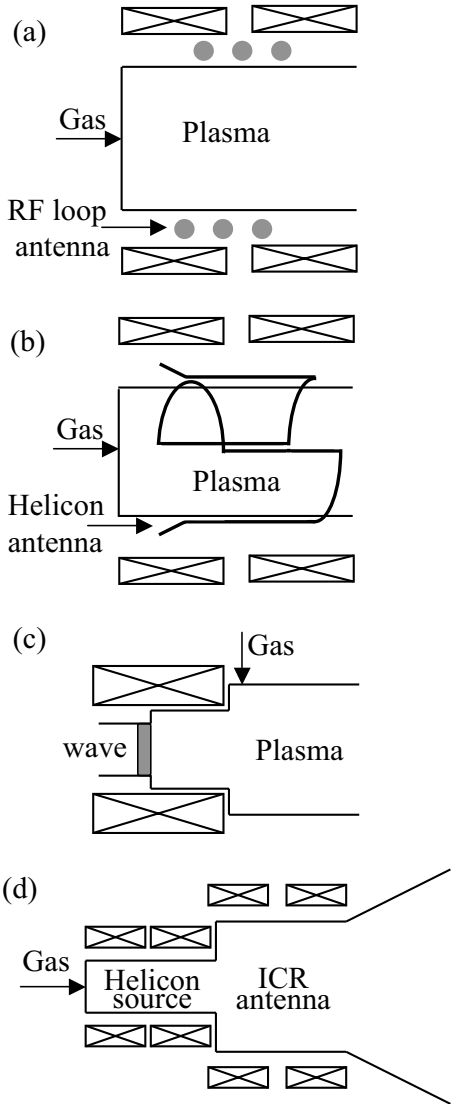

Figure 3. Schematic of the main 'plasma' thrusters: (*a*) RF plasma thruster, (*b*) HDLT, (*c*) microwave (ECR) plasma thruster, (*d*) Variable Specific Impulse Magnetoplasma Rocket (VASIMR); (*b*) and (*d*) operated with RF; ion cyclotron resonance (ICR); in (*a*) the RF loop antenna can be replaced by a 'stove top' antenna pushed against the left end of the plasma cavity as in the TCP inductive source (Lieberman and Lichtenberg 1994); (*a*) and (*b*) can be operated with or without solenoids and the latter can be replaced by permanent magnets.

3. Plasma basics for propulsion

An electric thruster typically comprises three components or regions as shown in figure 4: the plasma coupling region, the ion extraction/acceleration region and the ion beam neutralization/detachment region (or plasma plume). The latter two are often defined as the thruster exhaust. The main distinction between a gridded ion thruster and a plasma thruster is the use, or not, of electrically biased multi-aperture grids for the extraction and acceleration of the ion beam which then has to be neutralized. Gridded 'ion' thrusters (figures 2(*b*)–(*d*)) and electrode-less 'plasma' thrusters (figure 3) can be classified by their driving frequency which involves various power transfer mechanisms to the electrons. Common aspects

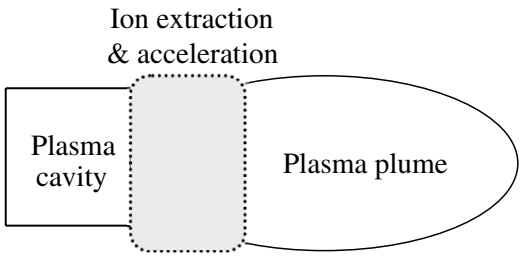

Figure 4. Schematic showing the three components of an electric thruster (plume neutralizer not shown).

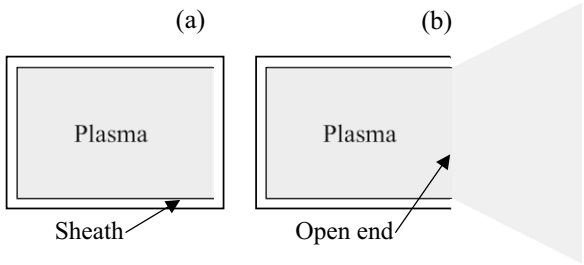

Figure 5. Schematic of a plasma in a (*a*) closed or (*b*) open to space cavity.

of plasma discharges and how they relate to thruster design will be presented first. Here we consider an idealized 'Maxwellian' plasma box (figure 5(*a*)) with an electropositive gas so that electrons are the only negatively charged particles and their distribution is that of a Maxwellian with a temperature, kT_e, much larger than the positive ion temperature, kT_i (Lieberman and Lichtenberg 1994).

3.1. Plasma cavity

3.1.1. Plasma sheaths and bulk plasma potential. To balance the flux of the mobile electrons and less mobile ions to the wall of the plasma cavity, thereby maintaining electroneutrality in the plasma bulk, a plasma establishes a thin 'positive' sheath at its boundaries ($V_s = \frac{kT_e}{e} \ln(M_i/2\pi M_e)^{1/2} \sim 4.7\ \frac{kT_e}{e}$ in argon for a width of the order of a Debye length λ_d), as shown in figure 6(*a*) (M_e is the mass of an electron). A 'presheath' with a potential drop of about 0.5 $\frac{kT_e}{e}$ also forms over a distance of about one ion–neutral collision mean free path (a few hundred Debye lengths) from the sheath edge to the plasma bulk to accelerate ions to at least the Bohm velocity $v_B = \sqrt{\frac{kT_e}{M_i}}$ at the presheath/sheath edge. Hence for grounded walls the plasma potential V_p will be about 5.2 $\frac{kT_e}{e}$ in argon. For insulating walls, V_p will shift up or down (usually up) by V_w, the wall potential (figure 6(*a*)). Wall charging occurs during the plasma breakdown phase before equilibrium is reached. This is often seen in low pressure inductively coupled magnetized plasma sources as the axial dc magnetic field limits the cross-field diffusion of electrons at low pressure (Charles and Boswell 1995a). In the wall sheath, the ion density is much larger than the electron density and the region is often called a 'single layer' or an 'ion sheath' as it contains mostly positive charges (Lieberman and Lichtenberg 1994, Hershkowitz 2005). The current density (or 'Bohm' current)

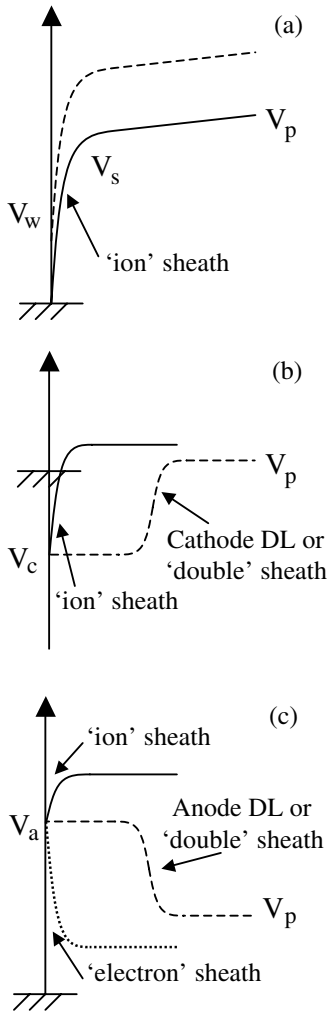

Figure 6. Schematic of various sheath and plasma potential profiles in contact with a: (*a*) wall, (*b*) cathode and (*c*) anode.

of ions entering the sheath is

$$I_i = n_s q v_B = 0.6 n_0 q v_B, \tag{8}$$

where q is the ion charge, n_0 and n_s are the bulk (or more accurately at the start of the presheath) and sheath edge density, respectively. Similarly, sheaths or potential gradients will develop at any object (grid, electrode) inserted in the plasma cavity. For example an ion sheath of amplitude $V \sim (V_p - V_c) \sim V_c$ will develop near a strongly negatively biased ($V_c \gg \frac{kT_e}{e}$) cathode inserted in the plasma cavity (figure 6(*b*)). Dc or RF bias is often used in the microelectronics industry for increasing the ion energy impacting a surface. The ion current density through the sheath is given by the Child–Langmuir equation:

$$I_i = \frac{4\epsilon_0}{9}\sqrt{\frac{2e}{M_i}}\frac{V^{3/2}}{d^2}, \tag{9}$$

where ϵ_0 is the permittivity of free space, e is the electron charge and d is the sheath thickness (Lieberman and Lichtenberg 1994).

The case of a positively biased anode inserted in the plasma cavity is of particular interest to thruster design

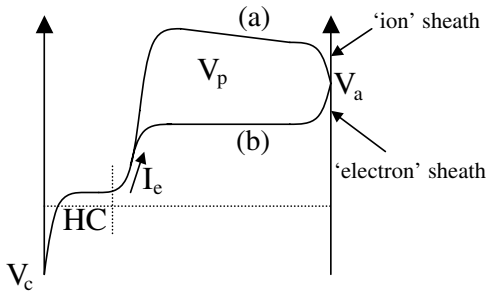

Figure 7. Schematic of the sheath and plasma potential profile inside the cavity of a dc electron bombardment ion thruster for a (*a*) large and (*b*) small area anode (HC = hollow cathode).

(figure 6(*c*)) as the sheath structure ultimately results from the positive ion and electron currents lost globally from the plasma. This includes all boundaries such as walls, electrodes, probes and grids. This will consequently determine the bulk plasma potential (Baalrud *et al* 2007) and other parameters such as the self-bias on an RF electrode (Smith *et al* 1997). When a positive bias V_a (relative to the plasma potential) is applied to an anode immersed in the plasma, an electron sheath forms and an electron current is drawn by the anode (dotted line in figure 6(*c*)). If V_a is increased, a bright 'anode' plasma forms in contact with the anode to increase the effective collection and supply a sufficient electron current. A double layer (DL), a strong potential drop over a narrow distance within a plasma (sections 3.1.1 and 3.2.3) is formed a few hundred Debye lengths from the anode (dashed line in figure 6(*c*)) and its amplitude is of the order of the ionization energy threshold of the gas ($e\phi_{dl} \sim E_i \sim 15$ V in argon); the sheath is then 'detached' from the anode and is called an anode DL (Baalrud *et al* 2007). To obtain an ion sheath in contact with the anode (the anode is still drawing an electron current but is 'decelerating' the electrons), the anode surface area has to be much greater to balance the discharge current (solid line in figure 6(*c*)). Here the anode is biased positively with respect to ground but negatively with respect to the plasma potential.

A typical dc-discharge electron bombardment ion thruster with a hollow cathode (HC), anode and first screen grid is shown in figure 2(*b*) (Goebel and Katz 2008). Most of the radial walls are essentially the anode and this large area anode configuration gives the typical operating potential profile (*a*) in figure 7, with an ion sheath near the anode. An operating profile such as (*b*) in figure 7 with an electron sheath near the anode (similarly to the dotted line in figure 6(*c*)) would be obtained by significantly reducing the anode area (and effectively adding grounded or insulating walls). Profiles (*a*) and (*b*) in figure 7 also show that electrons from the HC are accelerated by the potential difference between the cathode and the bulk plasma since the thruster design is usually optimized to have a bulk plasma potential near or slightly higher than the anode voltage ($V_p \sim V_a$). The cathode sheath can develop into a cathode DL formed a few hundred Debye lengths from the cathode (similarly to the anode DL) such that the bright plasma in contact with the cathode will draw a sufficient ion current (dashed line in figure 6(*b*)).

In summary, the plasma will self-bias in order to conserve charge. The sheath, bulk potential and density profiles will be dominated by space-charge effects. In addition to the plasma cavity geometry, applied dc magnetic fields using solenoids (divergent or radial fields) or permanent magnets (magnetic multipole fields or ring cusps fields) will affect radial and axial transport of charged particles and the effective boundary area (Goebel and Katz 2008, Charles 1993). Thruster optimization aims at maximizing the ion current extracted along the central axis and at minimizing radial loss. When electrodes are not in direct contact with the plasma, for example an antenna surrounding a glass tube, radiofrequency is used to couple the power to the plasma and an RF sheath forms between the plasma and the glass tube innerwalls. Overall, the properties of collisionless dc and RF sheaths are similar in the context of this study (Lieberman and Lichtenberg 1994, Manheimer 2000, Charles *et al* 2000). The bulk plasma potential may have a small RF component [$V_p = V_{dc} + V_{rf} \sin(wt)$] in the electron heating region which results from capacitive coupling which will be neglected here. Finally, the low pressure operating range of thrusters means that the sheath is collisionless and no energy is lost by ion–neutral charge exchange collisions in the sheath.

3.1.2. Simplified power balance. The idealized plasma shown in figure 5(*a*) can be produced in many ways and a first approach is to classify these plasmas and consequently the thrusters by their driving frequency: dc (continuous and pulsed), RF and microwave (figures 2(*b*)–(*d*) and figure 3). The type of excitation will influence the heating mechanism for the electrons and the resulting electron energy distribution function. Here a Maxwellian has been assumed for the electrons and the electron temperature can be obtained from particle balance of the ions, where the ion production rate equals the ion loss rate at steady state. To understand the basic plasma parameters which will effect the final thrust and specific impulse defined above, it is convenient to express the power loss from the charged particles and from radiation to the walls of the plasma cavity (figure 5(*a*)). At steady-state, the power input into a plasma cavity will balance the power lost on the walls which can be written as

$$P_{loss} = A_{sheath} q n_{sheath} v_i \left(V_p + E_i + E_e + \frac{2kT_e}{e} \right), \qquad (10)$$

where A_{sheath} is the wall sheath area (for high plasma densities and not so large sheath potentials, the sheath width is smaller than 1 cm and the wall sheath area is simply the area of the walls), n_{sheath} is the plasma density at the wall sheath, $v_i = v_B$ and is the Bohm velocity or ion sound speed and E_i and E_e are the ionization and excitation energy of the gas (Lieberman and Lichtenberg 1994, Charles *et al* 2003). For each ion leaving the plasma, an electron leaves and the average energy lost per electron that strikes the wall is $\frac{2kT_e}{e}$. Applied potential or current on electrodes/antennae generate electron heating and collisions with the injected gas to produce the positive ions, which are the main source of thrust. The cross-section for ionization by electron impact exhibits an energy threshold E_i and has the profile shown in figure 8 for argon. Unfortunately for the present application to electric propulsion, the cross-section for excitation of neutrals by electron impact has a

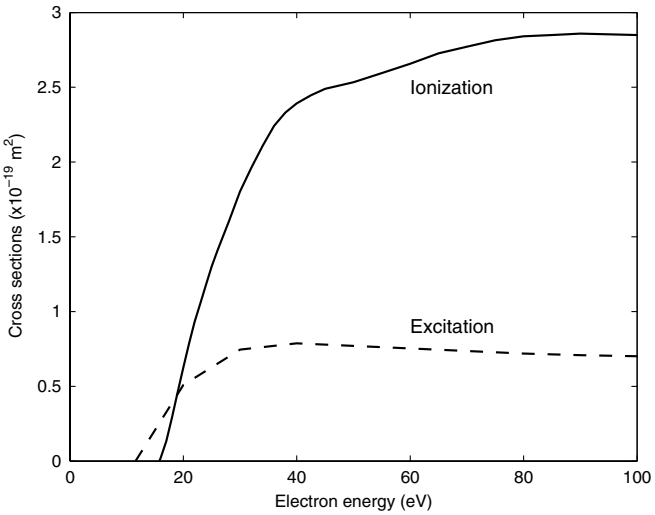

Figure 8. Ionization and excitation cross-sections in argon.

Table 1. Ionization potential E_i of various gases (www.chemglobe.org) (in increasing order of E_i, (†) metal), (⋆) inert gases).

Gas	E_i (V)
Caesium† (Cs)	3.9
Potassium† (K)	4.3
Xenon⋆ (Xe)	12.1
Molecular oxygen (O_2)	12.5
Nitrous oxide (N_2O)	12.9
Atomic hydrogen (H)	13.6
Atomic oxygen (O)	13.6
Carbon dioxide (CO_2)	14.0
Krypton⋆ (Kr)	14.0
Atomic nitrogen (N)	14.5
Molecular hydrogen (H_2)	15.4
Molecular nitrogen (N_2)	15.6
Argon⋆ (Ar)	15.7
Neon⋆ (Ne)	21.6
Helium⋆ (He)	24.6

similar amplitude, threshold E_e and energy range (shown in figure 8 for argon). Except for metastable atoms, excited atoms will return to lower energy states by emitting photons. The radiation is usually in the visible and ultraviolet and is a large source of power loss. Hence the minimum energy cost in creating an ion is about $e(E_i + E_e)$.

Doubly charged ions can also be produced by a second ionization collision ($e^- + X^+ \rightarrow X^{++} + 2e^-$ or $e^- + X \rightarrow X^{++} + 3e^-$) and the corresponding threshold potential is 27.7 V for argon and 21.2 V for xenon. The velocity of a doubly ionized ion is $\sqrt{2}$ times the singly charged ion velocity. The ionization potential, E_i, of various gases are shown on table 1 in increasing order. Mercury and caesium have the lowest ionization energy threshold (about 4 eV) and were the propellant of choice in early tests of ion gridded engines in space due to their maximum power efficiency, for example NASA's SERT 1 ion thruster flight test (Gold *et al* 1964). These have since been abandoned due to the hazards associated with handling them and the damage caused to sensitive spacecraft surfaces, like solar arrays, from contamination by these metals. Inert gases are the preferred choice. Since most inert gases (neon, argon, krypton and xenon) have similar ionization energy threshold (around 15 V). Equation (10) shows that for a constant value of P_{loss} an increase in mass will result in a decrease in velocity (equation (6)) and an increase in plasma density. Despite its cost as a result of its low abundance on Earth, xenon is the propellant of choice for electric propulsion in space as it is a high-mass inert gas with a relatively low ionization energy ($E_i = 11$ eV). It also has a low pressurized tank mass. Since there is a finite amount of xenon on Earth, any space mission removes some of that source forever.

3.2. Acceleration and extraction

Electric thrusters can also be classified in terms of the type of ion extraction and acceleration mechanism. Gridded ion thrusters use a system of biased grids (1 grid in contact with the plasma) and the plasma source can be dc, RF or microwave driven (figures 2(*b*)–(*d*)). Although Hall thrusters do not have grids, a dc potential difference is applied between an internal anode and the external cathode; the latter also serves as an electron provider for beam neutralization (figure 2(*e*)). Finally, ion acceleration with no immersed electrode (for the discharge coupling or for the ion acceleration) takes place in a plasma expansion (figure 3). Expanding plasmas have various degrees of complexity which depend on the electron heating mechanisms and on the expansion mode. Although initial designs for dc magnetic expansion thrusters have been discussed (Jahn 2006) here only RF and microwave plasma coupling are considered.

3.2.1. With grids (e.g. gridded ion thrusters). An ion beam can be extracted and accelerated from a plasma by using electrostatically biased multi-aperture grids: two to four grids can be used and the three grid configuration has been applied to the most successful ion thruster missions (Goebel and Katz 2008, Goebel 2008). The potential difference between the first grid (in contact with the plasma) and the 'last' grid (in contact with the plasma plume in the exhaust) defines the ion beam energy. The potential difference between the first grid and the second grid (with the accelerating potential) defines the shape of the sheath near each extraction hole in the grid and the fraction of current that can be extracted (equation (9)). The beam parameters are strongly coupled in the two grid configurations and adequate extraction is achieved for a limited beam energy range. Hence three grids are usually used (figure 9) where V_1, V_2 and V_3 are defined as the screen, accelerating and decelerating grid potentials. A better adjustment of extraction and acceleration is obtained. Details on ion optics can be found elsewhere (Goebel and Katz 2008). Briefly, the shape of the extracted ion beam (convergent, collimated or divergent) is strongly dependent on the shape of the sheath near the hole of the screen grid. From the Child–Langmuir law (equation (9)), the gap between the screen and the accelerating grids should be similar to the sheath thickness. The screen grid reduces the flux of ions 'missing' the holes of the accelerating grid (and being collected by the accelerating grid) and limits erosion of the accelerating

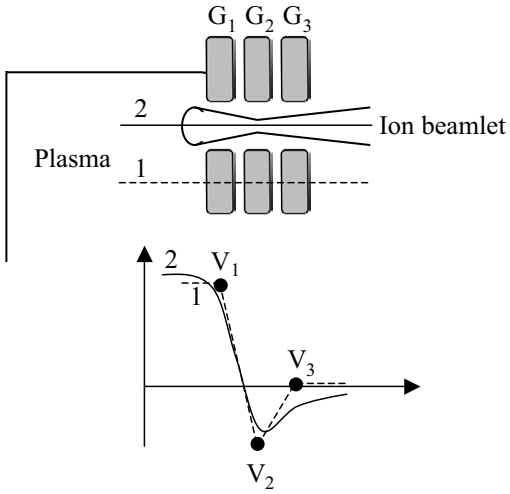

Figure 9. Schematic of the 3 grid extraction system in an ion gridded thruster showing one ion beamlet and the corresponding axial potential profile (not to scale).

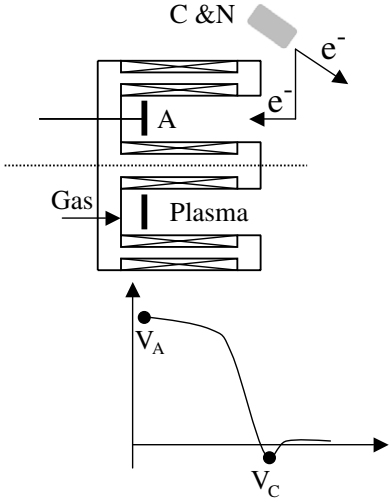

Figure 10. Schematic of the Hall thruster and its axial potential profile (not to scale).

grid. The third grid adds complexity to the ion optics but also largely reduces erosion of the accelerating grid: without the decelerating grid, cold ions produced by ion–neutral charge exchange collisions in the plasma plume would accelerate back towards the thruster cavity. The decelerating grid also allows an increase of ion beam density (via an increased bias on the accelerating grid) while maintaining a fixed exhaust velocity. Gridded ion thrusters with 2 or 3 grids have one stage only for both extraction (from the plasma) and acceleration (in the exhaust) and the maximum achievable beam energy is about 8 kV. Decoupling the beam acceleration from the beam extraction by adding a 4th grid would push this limit up to 80 kV beam energy. A maximum of 30 kV has been obtained in laboratory tests (2005 and 2006) at the European Space Agency development centre (ESTEC) of a dual stage 4 grid (DS4G) ion thruster prototype designed and built at the Space Plasma, Power and Propulsion laboratory at the ANU (Walker *et al* 2006, Bramanti *et al* 2009). A generalization of the Langmuir–Blodgett laws used for ion extraction with grids has been recently discussed (Sutherland *et al* 2005a) which shows the limits of equation (9). In summary, ion extraction and acceleration with grids is an effective method and plays a major role in the development of electric propulsion. The main factor which limits the lifetime of a gridded ion thruster is grid wear (e.g. erosion, arcing).

3.2.2. With electrodes (e.g. Hall thrusters). The literature on Hall thrusters, also called 'Closed drift' thrusters, is extensive (Zhurin *et al* 1999 and references therein, Goebel and Katz 2008). Experimental and theoretical studies started in the USSR in the 1960s and experienced a phenomenal effort in the late 1980s. Two types of Hall thrusters were developed, the 'magnetic layer' type and the 'anode layer' type. The magnetic layer Hall thruster is schematized in figures 2(*e*) and 10 and is the basis of missions such as SMART 1 (Goebel and Katz 2008). A potential difference V_d is applied between an anode and a cathode to create the discharge. A radial magnetic field is generated between the inner and outer poles and electrons flowing from the cathode to the anode interact with the radial field and produce ionization. Most electrons leaving the cathode go to the ion beam and neutralize it. The resulting potential along the exhaust axis is shown on figure 10 (Hass and Gallimore 2001, Raitses *et al* 2002, Taccogna *et al* 2008). The discharge channel is usually bounded by ceramic walls which provide low energy secondary electron emission to maintain a low electron temperature and extend the acceleration zone. Except in the region where the electron temperature can be high, the radial magnetic field lines are thought to be plasma equipotentials and consequently define the ion trajectories in the exhaust (Keidar *et al* 2004, Haas and Gallimore 2001, Fruchtman and Cohen-Zur 2006). The ceramic is subject to erosion which is the main limit in terms of thruster lifetime. Oscillations of discharge parameters exist and constitute a complex challenge (Zhurin *et al* 1999, Choueri 2001).

3.2.3. Without 'immersed' electrodes (e.g. expanding plasma thrusters).

(i) Gradual expansion. Expansion of a plasma into vacuum or a lower density background plasma leads to ion acceleration, a process studied analytically and experimentally with a variety of plasma diagnostics since the 1930s and described by various authors (Manheimer 2001 and references therein, Hairapetian and Stenzel 1991, Sack *et al* 1986, Kaganovich *et al* 1996, Charles *et al* 1991, Hussein and Emmert 1990, Yoon *et al* 2005, Lafleur *et al* 2009). As shown in figure 11(*a*), a geometric expansion from a small diameter plasma source to a larger diameter diffusion chamber (or to space) creates a pressure gradient along the expansion and an axial electric field sets up to retard the mobile electrons (and accelerate the ions) to maintain electroneutrality. This is similar to the sheath treatment detailed in section 3.1 but here the plasma cavity is open at one end as shown in figure 5(*b*). Assuming a constant electron temperature along the expansion leads to the Boltzmann relation

$$n(z) = n_0 \exp\left[\frac{e(V_p(z) - V_{p_0})}{kT_e}\right], \qquad (11)$$

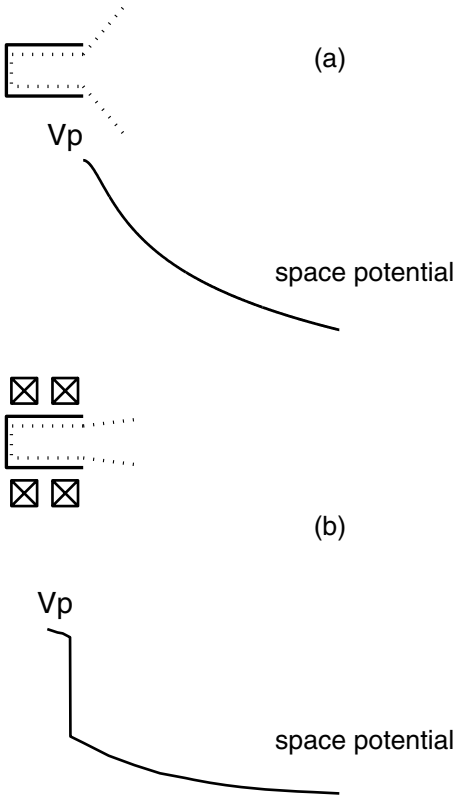

Figure 11. Schematic of the axial plasma potential profile for a (*a*) gradual expanding plasma and (*b*) an expanding plasma containing an electrostatic shock or DL (not to scale).

where n_0 and V_{p_0} are the plasma density and potential at the point source of the expansion, respectively. Plasma expansion of the solar wind into the universe is close to a 'spherical' expansion where

$$n(z) \sim \frac{n_0}{z^2}. \tag{12}$$

Near-spherical expansion can also be obtained in the laboratory when using small diameter sources and the resulting potential decrease has the shape shown in figure 11(*a*) (Charles *et al* 1991, 1992, Corr *et al* 2007, Hippler *et al* 2009). An important parameter is the operating pressure multiplied by the cavity diameter (or characteristic length). For a larger diameter source, the Boltzmann expansion will still be valid for regions away from the plasma creation zone, with or without the presence of an applied axial magnetic field (Charles and Boswell 2003, Aanesland and Charles 2006). Figure 12 shows a typical data set of density versus V_p on a semi-logarithmic scale and the determination of kT_e from the slope of the line of best fit (equation (11)) obtained in the 15 cm diameter CHI KUNG device (Charles 2007) with a magnetic field diverging from about 90 G to a few gauss. The electron temperature is found to be about 3.5 eV for an argon pressure of 3 mTorr. The plasma potential of 5.2 $\frac{kT_e}{e} \sim 18$ V corresponds to the axial position where the plasma 'connects' to ground and the floating potential measured at that axial position is zero. This plasma is very close to the 'standard' case of section 3.1 and figure 5, mostly because the gas pressure is sufficient for thermalization processes to occur. Here there is a combination of a geometric and magnetic expansion. Fast ions, sometimes

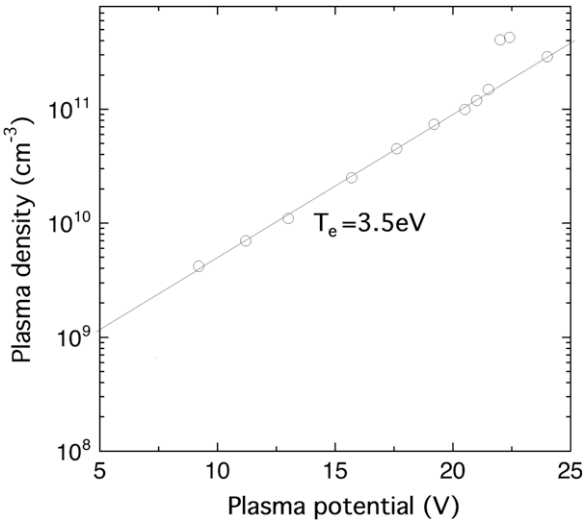

Figure 12. Example of a laboratory Boltzmann expansion obtained in the 30 cm long 15 cm diameter CHI KUNG source (Charles 2007) operating at 500 W, 3 mTorr in argon and with a magnetic field diverging from a maximum of 90 G ($z = 25$ cm) to 9 G ($z = 45$ cm). T_e is derived from the slope.

forming a beam with a low energy spread, will be seen at low pressure ($\leqslant$2 mTorr in argon) over a distance of about a few ion–neutral collisional mean free paths (Charles *et al* 1992, Corr *et al* 2007) but a divergence as high as 45° from the central axis is measured (Corr *et al* 2008).

(ii) expansion with electrostatic shock. Non-linear phenomena such as collisionless electrostatic shocks or electric DLs can appear along a plasma expansion (Charles 2007). For example, the expansion of figure 11(*b*) can be obtained with a divergent magnetic field (with sufficient ion confinement for a particular plasma source diameter) and for pressures less than a few millitorr (Charles and Boswell 2007). Ion acceleration across the shock results in the formation of a large area collimated ion beam. The electric field of DLs and resulting accelerated ion beams have been detected in the Earth's aurora using probes on satellites (Ergun *et al* 2004). In the laboratory, the expansion along z from the low potential edge of the DL is a Boltzmann expansion if ionization is not predominant in that region (figure 11(*b*)). Although the Boltzmann relation could be verified in some DLs, in many cases DLs can be sustained without a much reduced density (Hershkowitz 1985). From equation (11) a Boltzmann DL with $\Delta\phi_{dl} = V_{up} - V_{down} = 25$ V and $kT_e = 8$ eV would yield $\frac{n_{up}}{n_{down}} \sim 23$ where V_{up}, V_{down}, n_{up} and n_{down} are the plasma potential and plasma density at the upper and lower edges of the DL, respectively. In the CHI KUNG expanding DL device (described in section 5), a ratio $\frac{n_{up}}{n_{down}}$ of 1 or 2 is typically measured which does not follow equation (11) (Charles and Boswell 2003, Lieberman and Charles 2006). Such DL solutions can be found by assuming various charged particle populations (Andrews and Allens 1971), the most common being the 4 populations scenario schematized in figure 13: trapped and free electrons, thermal and accelerated ions. A variation of such a model with a 5th species (electron beam accelerated from downstream to upstream) gives DL solutions for a

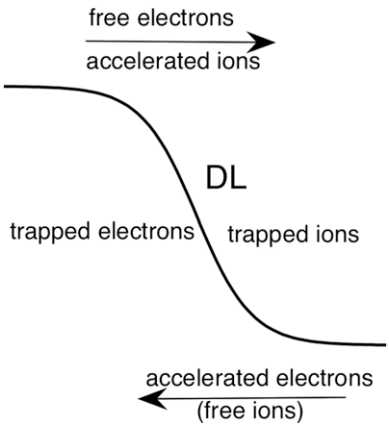

Figure 13. Schematic of a DL showing the four charged particle populations, the trapped and free electron populations and the accelerated and thermal (trapped) ion populations.

current-free DL (Lieberman *et al* 2006). None of these models includes the presence of a magnetic field. A direct application of the laboratory current-free 'expanding' DL for spacecraft propulsion will be detailed in section 5.

3.3. Neutralization and detachment of the plasma plume

The accelerated ion beam must be neutralized to form a plasma plume in order to detach from the spacecraft, thereby providing thrust, and to prevent spacecraft charging and stalling of the ion beam due to its own space charge. Interaction of this plasma plume or of some of its components with the spacecraft components (e.g. solar arrays, electronic sub-systems) will be detrimental to the spacecraft operation and lifetime. Thrusters using grids or immersed electrodes use an external HC to emit electrons which neutralize the ion beam. Electrode-less plasma thrusters do not require an external neutralizer as a neutral plasma containing energetic ions is emitted (at least in principle). The plasma plume contains not only the energetic ions and the neutralizing electrons, but also any non-ionized propellant gas, and low energy ions resulting from charge exchange between the beam and the non-ionized gas (from the thruster cavity or from the HC neutralizer) or from local ionization of the non-ionized gas. Sputtered thruster material (usually in the form of neutral atoms or molecules) may also be present and is of major concern to, e.g., solar panels if metallic. A simple experimental approach is to spatially measure the ion energy distribution function in the exhaust as this is the main component of the thrust. The most divergent part of the plume is often responsible for spacecraft damage. The plume optical emission is very weak and the corresponding radiation loss is very small. The main difference between plume characterization in a laboratory experiment (thruster contiguously attached to a vacuum chamber), a prototype experiment (thruster immersed in a large space simulation chamber) and an experiment on a spacecraft (thruster operating in space under limited operating conditions with limited plume diagnostics) is the background gas pressure (Goebel and Katz 2008).

An energetic ion beam 'decays' or loses its energy by charge exchange collisions with neutrals. Directionality is not lost and the hot neutrals conserve the 'thrust'. However, the plume signal to be measured usually decays exponentially with distance and the mapping is limited to about one ion–neutral collisional mean free path (Lieberman *et al* 2006, West *et al* 2008). The charge exchange collision cross-section at ion energies ranging from 0.1 to 100 eV is about 10 to 2×10^{-19} m^2 in xenon and 7 to 3×10^{-19} m^2 in argon, respectively (Scott Miller *et al* 2002, Okuno *et al* 1978, Pullins *et al* 2000, Lieberman and Lichtenberg 1994). Typically at 1 mTorr in argon, the mean free path for a charge exchange (elastic) collision is 4 cm (4.6 cm) for a 0.01 eV ion and 8.2 cm (10.6 cm) for a 20 eV ion; the mean free path using the sum of both ion–neutral collision cross-sections is 2.1 cm for a 0.01 eV and 4.6 cm for a 20 eV ion.

Models of the plasma plume in the exhaust of gridded dc ion thrusters and Hall thruster exist (Goebel and Katz 2008). Often laboratory experiments do not provide adequate data and the physics behind neutralization and detachment is complex especially for expanding magnetized plasma thrusters with the added complexity of an applied expanding dc magnetic field and the presence of a 'downstream' plasma in the laboratory and possibly in space (Hooper 1993, Gesto *et al* 2006, Gesto *et al* 2008, Arefiev and Breizman 2005, Deline *et al* 2009). The physics of the plume is largely unknown but successful electric propulsion missions have clearly demonstrated that plume detachment from the thruster occurs and that thrust is generated.

4. Inductively coupled and wave-excited plasma sources, e.g. the helicon source

In low pressure high density inductively or wave-excited plasma sources, RF or microwave power is coupled to the plasma across a dielectric as opposed to via an immersed electrode. Compared with capacitively coupled plasmas, the wall sheath potential is lowered from a few hundred volts to a few tens of volts (Lieberman and Lichtenberg 1994). Although this decrease in potential may not be attractive for propulsion these sources can achieve very high densities at low pressure. Applying electron cyclotron resonance (ECR) plasma sources based on figure 3(*c*) (Jahn 2006, Manheimer 2001) and RF plasma sources based on figures 3(*a*), (*b*) (Chang-Diaz 2000, Charles and Boswell 2003, 2008 Cohen *et al* 2003, Charles *et al* 2006, 2008a) to electric thrusters has been discussed but to date there is no mature electrode-less thruster technology based on these low pressure high density plasmas. A combination of an electron RF heating stage with an ion cyclotron resonance heating stage has been proposed for VASIMR and is schematized in figure 3(*d*). VASIMR has been designed as a high magnetic field and high power plasma rocket with tens of kilowatts of input power. Various aspects of VASIMR have been discussed (Chang-Diaz 2000, Arefiev and Breizman 2004, Boswell *et al* 2004, Bering *et al* 2008). Specific studies of the ion cyclotron resonance heating have been carried out in a supersonic plasma flow produced by an MPD arcjet (Inutake *et al* 2007). Here for simplicity we use the example of a radiofrequency helicon source based on figure 3(*b*) to discuss how low pressure high density electrode-less plasma sources could operate as electric thrusters.

4.1. Plasma density and ionization rate

Helicon wave generated plasmas were first produced in the late 1960s by Boswell (Boswell 1970, 1974, 1984a, 1984b) in a 5 cm diameter (and a 10 cm diameter) 55 cm long (120 cm long) glass tube surrounded by two solenoids producing fields up to 2 kG: transverse RF fields excited by an external antenna wrapped around the glass tube were shown to launch helicon waves inside the low pressure argon plasma (typically 20 mTorr in the small diameter tube and 1.5 mTorr in the large diameter tube). The antenna length and geometry was set to resonantly excite the helicon waves and the measured electron density would undergo discrete upward jumps (hence achieving higher efficiency in plasma production) with increasing magnetic field (for a constant power) or increasing RF power (for a constant field) as shown in subsequent work (Boswell and Porteous 1987). Various tube lengths and diameters as well as various antenna geometries (later defined as 'Boswell' or double-saddle-field antenna, double-half-turn antenna, single loop antenna, Nagoya antenna) have since been used in helicon experiments worldwide (Boswell and Chen 1997, Chen and Boswell 1997). The wave propagation depends on the radial density plasma profile and on the boundary conditions (Boswell 1984a) and these plasma sources are known as 'helicon' sources. One attractive feature of the helicon source (as opposed to 'standard' ECR sources which require high magnetic fields for adequate operation) is that it does not have to run in a resonant wave mode and can operate under a broad range of plasma coupling modes with a broad range of external parameters (pressure, RF power, RF frequency, dc magnetic field, geometry). It can also be easily scaled up or down in power and size and can be easily operated in the capacitive or inductive modes in the absence of any applied magnetic field (Charles *et al* 1992, Corr *et al* 2007). Helicon sources with permanent magnets around the glass tube or downstream of the glass tube have been described in detail (Virko *et al* 2007, Chen 2008, Takahashi and Fujiwara 2009, Boswell *et al* 1989, Charles 1993). In the early helicon experiments, ionization close to 100% was reported on the central axis for only 180 W input power in the 10 cm diameter tube operating at 1.5 mTorr of argon (Boswell 1984b) and densities greater than 10^{13} cm^{-3} were obtained in the 5 cm diameter tube at a few millitorr of argon using less than 1 kW (Boswell *et al* 1982). Densities in the 10^{12} cm^{-3} range can be obtained for low RF power (a few tens of watts) in smaller diameter sources (Toki *et al* 2006).

As an exercise, it is interesting to estimate the thrust from the ions (T_i) generated by an argon plasma at 1.5 mTorr of density $n_i = 10^{12}$ cm^{-3} (10^{18} m^{-3}), potential $V_p = 20$ V and electron temperature $kT_e = 3$ eV emitted at one end of a 10 cm diameter glass tube (figure 5(*b*)):

$$T_i = v_{i_{ex}} \frac{d(m_i)}{dt} = v_{i_{ex}} (n_i v_B A M_i), \tag{13}$$

where $A = \pi R_{tube}^2$ is the tube cross-section area (80×10^{-4} m^{-2}), v_B is about 2700 m s^{-1} and $v_{i_{ex}} = \sqrt{\frac{2qV_p}{M_i}} \sim 9800$ m s^{-1} (it is assumed that the space potential at infinity is zero and that the plasma will detach from the tube). T_i is about 14 mN for 180 W (the power into the solenoid is not considered in this calculation). The thrust T_n obtained by simply ejecting the propellant can be estimated from equation (4) using $v_n \sim 300$ m s^{-1} and $n_n = 4.95 \times 10^{19}$ m^{-3} of argon atoms (pressure of 1.5 mTorr, temperature of 293 K). T_n is about 0.6 mN, which is very small compared with T_i. In the laboratory experiments, pumping speeds are typically a few tens to a few hundred litres per second and a pressure of 1.5 mTorr would typically correspond to an input flow rate of a few sccm. For a pumping speed of 300 L s^{-1} and a volume of 30 L, the residence time of each argon atom is about 100 ms. Assuming a neutral velocity of $v_n \sim 300$ m s^{-1} gives a distance of 30 m before an atom is actually pumped out of the system. Hence the flow is molecular and argon atoms re-enter the source multiple times and the same atom can be reused many times. At 1.5 mTorr the collision mean free path for argon atoms colliding with argon atoms is $\lambda = \frac{1}{n_n \sigma} \sim 20$ cm (using a cross-section σ of 10^{-15} cm^2), which is smaller or of the order of the size of the plasma source and diffusion chamber. In space, the exit of a 10 cm in diameter tube would be a black hole and the flow rate necessary for maintaining a pressure of 1.5 mTorr can be estimated using equation (3): $\Gamma_n = 1.785 \times 10^{21}$ atoms per minute which is 67.5 sccm or 2 mg s^{-1} of argon at 273 K.

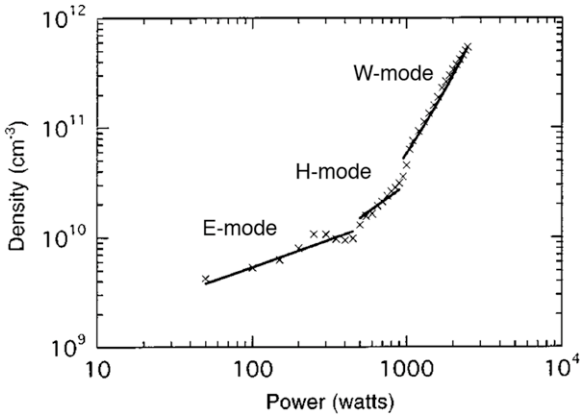

Figure 14. Schematic of plasma density versus RF power in a helicon source (Degeling *et al* 1996), showing the capacitive (E), inductive (H) and wave (H) modes; operating pressure are 3 mTorr (argon), 50 G. The two mode transitions are often accompanied by stronger density jumps (Perry *et al* 1991, Perry *et al* 2002). (Reprinted with permission from Degeling *et al* 1996, copyright American Institute of Physics.)

Figure 14 shows the density mode jumps in a helicon source with increasing RF input power and constant magnetic field. This was measured in the much larger WOMBAT apparatus with the probe in the diffusion chamber (Degeling *et al* 1996). Three modes of RF power coupling are identified: the capacitive coupling mode E ($n_e \leqslant 10^{10}$ cm^{-3} and $n_e \sim \sqrt{P_{rf}}$), where the power is input to the plasma through oscillations in the sheath (resonant circuit with RF voltage on the antenna), the inductive coupling mode H ($n_e \leqslant 10^{11}$ cm^{-3} and $n_e \sim P_{rf}$), where the power is input to the plasma within the skin depth of the antenna near field (resonant circuit with RF current flowing through the antenna), and the wave coupling mode W ($n_e \geqslant 10^{11}$ cm^{-3} and $n_e \sim \exp P_{rf}$), where plasma production occurs in the central axial region of the plasma body via the helicon wave. The RF power for which the

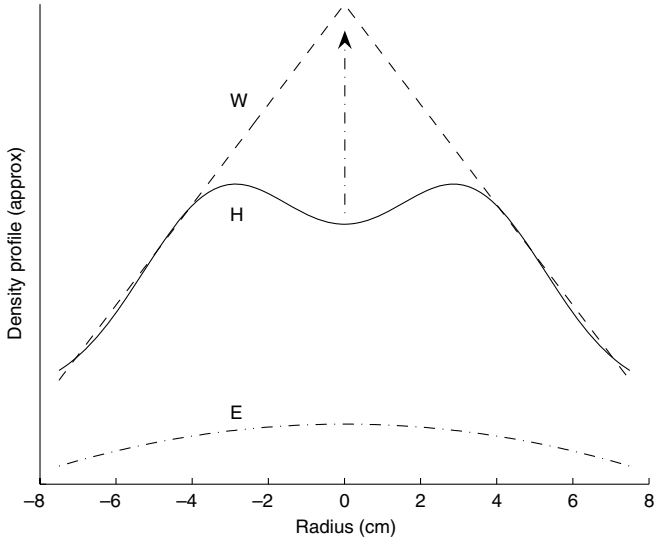

Figure 15. Schematic of the plasma density radial profile for the 3 coupling modes shown in figure 14, cosine (E), bi-modal (H) and triangular (W). Here a source diameter of 15 cm similar to that of the CHI KUNG device is used (Charles 2007).

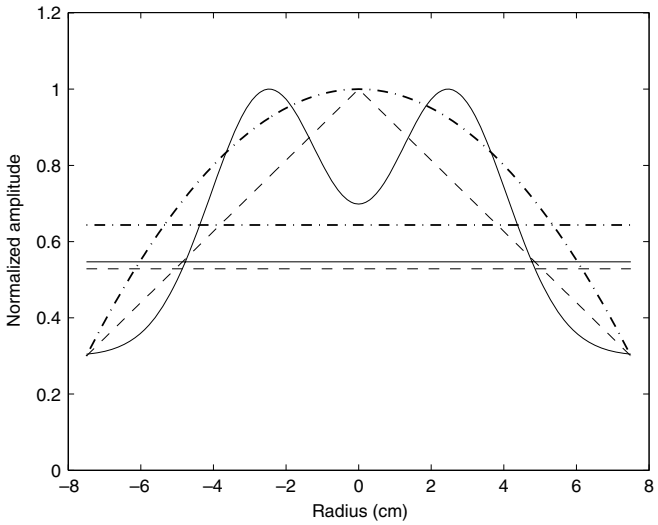

Figure 16. Schematic of typical normalized plasma density profiles for the E (dotted line), H (solid line) and W (dotted–dashed line) modes and their corresponding thrust coefficient (horizontal lines) integrated across a cylinder of diameter 15 cm (equation (14)).

E to H and H to W transitions occur vary with the helicon source geometry (the diameter in particular) and is typically 100–500 W and 500–800 W, respectively. More discrete jumps at higher rf powers corresponding to various wave modes and wave trapping mechanisms can be seen (Porteous and Boswell 1987, Perry *et al* 1991, 2002, Degeling *et al* 1996, Chi *et al* 1999, Sheridan and Chi 2000). Although not shown here, high β plasmas and very high densities $n_e \geqslant 5 \times 10^{12}\,\mathrm{cm}^{-3}$ can be achieved (Corr and Boswell 2007, Denning *et al* 2008). For example the 'blue core' is a low pressure plasma with a peak density of a few $10^{13}\,\mathrm{cm}^{-3}$ downstream of the helicon source where the magnetic field is applied; ion pumping ensures that neutrals are eliminated from this region and inhibits the density from rising further in the steady state. Greater power input results in higher ionization states. These effects can be observed in the source region only or in the diffusion chamber only depending on the magnetic field configuration. Radial loss is minimized and the principal plasma loss mechanism is plasma diffusion out the two ends of the source (Boswell 1984b). In the presence of a fully ionized core plasma, gas pumping effects are observed (Boswell 1984b). It should be noted that the energy cost of higher ionization states leads to considerably greater radiation loss than that expressed in equation (10) and should be avoided in thruster design. In fusion plasmas this is called radiation cooling. The cross-sections for excited levels of argon and xenon ions can be found in the literature (Strinic *et al* 2004, Man *et al* 1993).

4.2. Radial density profile and thrust reduction

In a helicon source, the ionization rate is not constant over the plasma cavity volume and the various coupling modes are usually associated with various radial profiles as shown by figure 15 (Boswell 1974, Degeling 1999). These profiles include a bell shape driven by ambipolar diffusion in the capacitive mode (with or without an applied magnetic field) and approximated by a cosine (diffusion in a slab where $n(r) \propto \cos\frac{2r}{\pi R_{\mathrm{tube}}}$); a bi-modal 'camel hump' shape in the inductive mode (with or without an applied magnetic field) approximated by the sum of 3 Gaussians, and a triangular shape in the wave mode (in a magnetized plasma with helicon waves). Here, for simplicity of comparison, a bulk to sheath density ratio of about $(1/0.3) \sim 3.3$ similar to that obtained in a free fall model in a cylinder of length a few tens of centimetres is assumed (Lieberman and Lichtenberg 1994) as shown in figure 16. This ratio varies greatly (from 1 to 10) with operating conditions and with position along the axis especially in the wave mode (Boswell 1974, 1984b, Degeling *et al* 1996, Degeling 1999, Sheridan and Chi 2000). For the bi-modal inductive mode, the depth of the central dip has also been arbitrarily chosen to be close to 20%. A cylinder diameter of about 15 cm similar to the HDLT plasma source detailed in section 5 is assumed. Using these profiles, equation (13) can be rewritten as

$$T_{\mathrm{i_{cyl}}} = v_{\mathrm{i_{ex}}} v_{\mathrm{B}} M_{\mathrm{i}} \left[2\pi \int_{r=0}^{R_{\mathrm{tube}}} n_{\mathrm{i}}(r) r \, \mathrm{d}r \right], \qquad (14)$$

where r is the tube radial axis and $T_{\mathrm{i_{cyl}}}$ is the thrust convoluted over the cylindrical cross-section and a fraction of T_{i} defined in equation (13). The capacitive, inductive and wave mode ratios $\alpha_{\mathrm{E,H,W}} = \frac{T_{\mathrm{i_{cyl}}}}{T_{\mathrm{i}}}$ between $T_{\mathrm{i_{cyl}}}$ from equation (14) and T_{i} from equation (13) are found to be about 0.65, 0.55 and 0.62, respectively (horizontal lines on figure 16) and do not vary much with R_{tube}. Hence for the plasma used as an example in the previous section, the thrust from ions exiting the 10 cm diameter cylindrical source is $\alpha_{\mathrm{W}} \times 14$ mN, which is about 9 mN for 180 W of input power.

4.3. Expansion and plume divergence

As mentioned previously, opening the plasma cavity (figure 5(*b*)) and assuming the Boltzmann expansion of

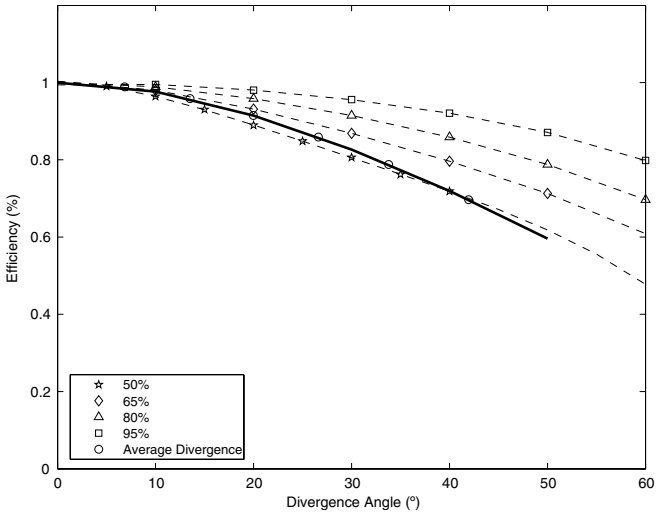

Figure 17. 2D calculation of the momentum efficiency versus ion beam divergence angle using a Gaussian beam profile and following a previously detailed method of divergence analysis (Cox *et al* 2008a).

figure 11(*a*) leads to divergence of the emitted plasma plume and therefore a loss in momentum efficiency. A quick estimation of this loss in two dimensions only is plotted in figure 17 assuming a plume with a Gaussian profile expanding with a divergence angle θ, for various percentages of the beam density calculated from the exhaust axis. This is carried out using a previously described method of divergence analysis (Cox *et al* 2008a) and the efficiency is invariant with the exhaust diameter or initial width of the Gaussian profile. For a divergence of 45° the average efficiency α_θ is about 0.65 and the thrust exiting the 10 cm diameter example is now reduced to $\alpha_\theta \times \alpha_W \times 14$ mN which is about 7 mN (180 W). Here it is assumed that all other parameters are kept constant. This effect is valid for all types of electric thrusters and has been previously documented (Goebel and Katz 2008). For a collimated ion beam such as that generated with an electrostatic shock (figure 11(*b*)), the average divergence is less than 10° and α_θ is close to 1 (Cox *et al* 2008a) as detailed in section 5.2.

4.4. Source wall charging

Equation (13) shows that the thrust will increase with an increase in electron temperature and/or plasma potential (increase of v_B and $v_{i_{ex}}$). The plasma potential in a Maxwellian ($kT_e = 3$ eV) argon plasma bounded by grounded walls is $V_p \sim 5.2\frac{kT_e}{e} \sim 16$ V which is near or just above the ionization potential in argon (table 1). The Bohm velocity is 2700 m s^{-1} and the velocity of an ion starting in the bulk plasma and accelerated in the wall sheath is about 9000 m s^{-1} (equation (6)). If an ion is extracted at the wall, its exhaust velocity can be increased by increasing the plasma potential. This can be achieved by reducing the operating pressure and hence increasing the electron temperature (Lieberman and Lichtenberg 1994), by increasing the wall potential V_w thereby giving a positive reference to the plasma (Charles 2005a, Meige *et al* 2005a, Lieberman *et al* 2006), by immersing an electrode inside the plasma to alter the loss area and/or alter the electron temperature (Aanesland *et al* 2003, 2004), by pulsing the plasma to select the breakdown phase which exhibits higher plasmas potentials (Boswell and Vender 1995, Charles and Boswell 1995b, 1998, 2004a, Smith *et al* 1997, Charles 2003) or by 'forcing' an expansion or density gradient via a change in source cavity geometry and/or magnetic field configuration (Charles and Boswell 2007, Corr *et al* 2007) and/or gas type (Plihon *et al* 2005, Charles *et al* 2008b). Typical values in the 50–100 V can be obtained for the plasma potential which gives a maximum exhaust velocity range from (15 to 22) $\times 10^3$ m s^{-1} in argon if detachment can be achieved and if the potential in space is assumed near zero. Wall charging has been studied in reactive plasmas used for plasma deposition of thin films (Charles and Boswell 1995a). The type and surface area of the plasma boundaries (insulating, conducting, grounded) will affect both the plasma breakdown phase (Smith *et al* 2003, Boswell and Vender 1995) and the final bulk plasma potential at steady state (Charles 2002, Aanesland *et al* 2005). It has also been shown that charging of the wall occurs during the plasma breakdown phase (Charles and Boswell 1995a). Hence thruster design can largely benefit from studies of wall effects, as demonstrated for Hall Thrusters (Zhurin *et al* 1999).

5. The HDLT

5.1. Concept

The HDLT is based on the formation of an electric DL, a strong drop of potential over a narrow distance within a plasma, in the thruster exhaust region (figure 11(*b*)). The electric field of the DL accelerates the ions created in the plasma cavity along the exhaust axis. A low divergence energetic ion beam, the main source of thrust, is emitted for DL operating conditions in argon of less than about 2 mTorr in pressure, an applied divergent magnetic field higher than 50 G in the plasma cavity, and a RF power larger than about 30 W for a plasma cavity of diameter 15 cm and length 32 cm. Although not a requirement for DL formation, if the source walls are fully insulating the DL is current-free. The ion beam is neutralized by the population of free electrons shown in figure 13 which overcome the potential barrier of the DL (Takahashi *et al* 2007). For a very low magnetic field (Charles and Boswell 2007) or a higher operating pressure (Charles 2003) a simple plasma expansion is obtained (figure 11(*a*)). The first HDLT propotype (Charles and Boswell 2002) was manufactured at the ANU and tested at ESTEC in 2005 and is based on the research experiment CHI KUNG (Charles 2007). The latter can be operated as a helicon source with large plasma densities associated with helicon waves by modifying the magnetic field configuration (Chi *et al* 1999, Sheridan and Chi 2000). With the presence of the DL, a linear increase in the ion beam density with increasing RF power is measured which would suggest operation in an inductive mode (H mode of figure 15). Here this mode is accompanied by large plasma potentials in the source (50–100 V) and some positive wall charging (10–30 V) (Charles 2005a, Meige *et al* 2005a, Lieberman *et al* 2006, Charles 2007). The HDLT is electrode-less and has no moving parts, hence it can be expected to have an extended lifetime.

The DL is formed during plasma breakdown and is stable and stationary afterwards (Charles 2005a). Hence both pulsed and continuous operation mode could be used in space missions. This type of plasma source can be easily scaled up or down in size and power (Sutherland *et al* 2005b, Byhring *et al* 2008) while maintaining the flexibility of operating in various plasma coupling modes to suit mission requirements (specific impulse and thrust). Scaling of the DL by orders of magnitude has been discussed (Boswell *et al* 2006).

5.2. Ion dynamics

The ion dynamics in an expansion with an electrostatic shock has been investigated in a number of expanding plasma devices worldwide (Charles and Boswell 2003, Cohen *et al* 2003, Sun *et al* 2005, Plihon *et al* 2005, Takahashi *et al* 2009). Upstream of the DL, there is one population of thermal ions and downstream of the DL, two ion populations are present: the accelerated ion beam and the thermal ions (figure 13). These populations have been measured experimentally using electrostatic probes (Charles and Boswell 2004a, 2004b, Charles 2005a, 2005b) and laser induced fluorescence (Sun *et al* 2005, Keese *et al* 2005, Cohen *et al* 2006, Biloiu *et al* 2005) and have been diagnosed in particle in cell computer simulations (Meige *et al* 2005a, 2005b) as well as in analytical models (Lieberman *et al* 2006, Lieberman and Charles 2006). The DL is located just inside the plasma cavity in argon in the CHI KUNG experiment (Charles and Boswell 2003) and extends across the entire source tube diameter as shown in figure 18 (Charles 2005b). The beam divergence has been recently measured by carrying out a spatial study in the plasma exhaust (figure 19) and a momentum efficiency of 98% has been obtained (Cox *et al* 2008a). Experiments with increasing pumping speed ranging from 50 to 1200 L s^{-1} have been carried out in the CHI KUNG device showing that the ion beam characteristics remain unchanged. With the HDLT prototype immersed in a vacuum chamber (effective pumping speed of 300 L s^{-1}), the ion beam has been recently diagnosed in argon (West *et al* 2008). The ion beam has been experimentally measured in the CHI KUNG device using xenon in agreement with analytical model predictions (Charles *et al* 2006, Charles and Boswell 2008). A high density xenon mode was found during the testing campaign at ESTEC (Charles *et al* 2008a). Experimental and computational plasma detachment studies have shown that the ion beam detaches about 10–15 cm downstream of the DL (Gesto *et al* 2006, 2008, Cox *et al* 2008a). Recent measurements in CHI KUNG have shown that the DL formation requires the presence of the expansion and the role of the downstream plasma is still largely unknown. The effect of external parameters such as propellant flow rate, gas pressure, RF power, magnetic field and plasma cavity geometry on the DL and ion beam characteristics have been discussed (Charles 2007, West *et al* 2008). Other aspects such as effect of frequency (Chakraborty Thakur *et al* 2009), instabilities (Aanesland *et al* 2006a, 2006b) have also been discussed. Detailed spatial studies are also reported (Cox *et al* 2008b, Biloiu *et al* 2008).

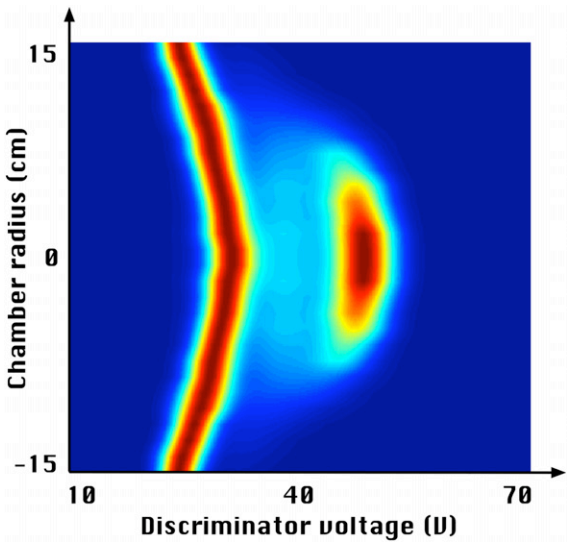

Figure 18. Normalized IEDFs obtained in the CHI KUNG device (Charles and Boswell 2004a, 2004b, Charles 2005a, 2005b) with the RFEA located 12 cm downstream of the DL showing the thermal ion population around the local potential downstream (about 30 V) and the higher energy ion beam (50 V). (Reprinted with permission from Charles 2005b, copyright 2005 IEEE.)

The physics of the current-free DL is non-linear and not yet fully understood and the thrust from ions could be initially written as

$$T_\mathrm{i} = v_{\mathrm{i_{ex}}} \frac{\mathrm{d}(m_\mathrm{i})}{\mathrm{d}t} = v_{\mathrm{i_{ex}}} (n_\mathrm{i} v_{\mathrm{intoDL}} A M_\mathrm{i}), \qquad (15)$$

where $v_{\mathrm{i_{ex}}} = \sqrt{\frac{2qV_\mathrm{p}}{M_\mathrm{i}}} \sim 17000\,\mathrm{m\,s^{-1}}$ is the ion exhaust velocity using a plasma potential V_p of about 60 V measured just upstream of the DL and v_{intoDL} is the velocity of the ions entering the DL. Analysis of this 'presheath' acceleration just upstream of the DL has shown measured ion velocities ranging from one to two times v_{Bohm} using laser induced fluorescence and retarding field energy analysers (Charles *et al* 2000, Rudakov *et al* 1999), v_{Bohm} in the particle in cell simulation and 1.3 v_{Bohm} in the theory. In addition, due to the lower pressure and complex electron dynamics, the electrons upstream of the DL are usually hotter than the standard 3 eV temperature of a 3 mTorr plasma (figure 12) and a v_{Bohm} of about 4400 m s^{-1} is calculated using a measured upstream temperature of 8 eV. Although thrust estimation from plasma parameters are useful, accurate measurements of thrust can only be determined by mounting the thruster on a properly designed thrust balance with the system operating in a space simulation chamber with adequate pumping capabilities. Alternative low cost techniques based on the displacement of a target plate hung as a pendulum and immersed in the thruster exhaust may be envisaged (West *et al* 2009).

5.3. Electron dynamics

The earlier assumption of a plasma with Maxwellian electrons (constant kT_e in the plasma cavity and along the exhaust axis) is inappropriate for a DL containing expanding plasma. As shown in figure 13, upstream of the DL, two electron

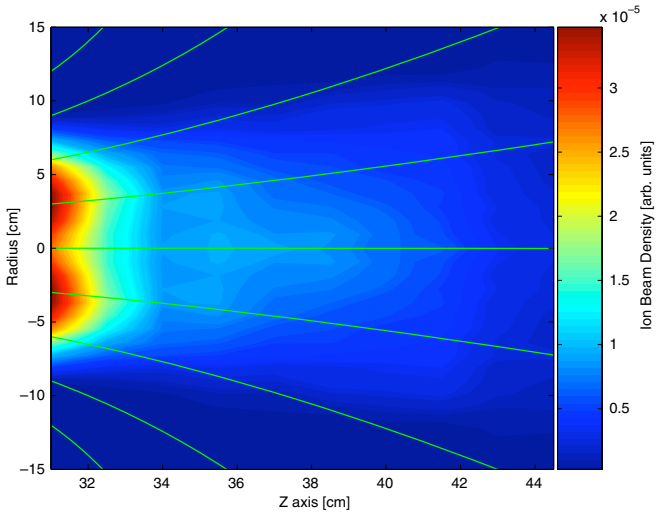

Figure 19. Spatial mapping of the ion beam density measured with the RFEA in the CHI KUNG device. (Reprinted with permission from Cox *et al* 2008a, copyright American Institute of Physics.)

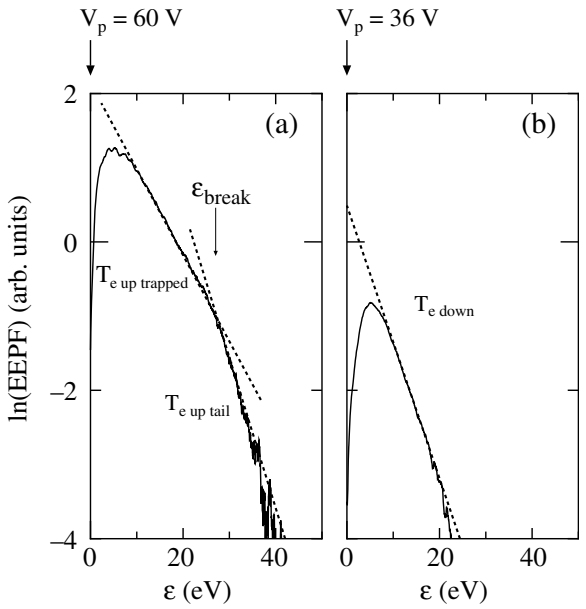

Figure 20. EEPF measured (*a*) 8 cm upstream of the DL in the CHI KUNG device showing the trapped and free electron populations and (*b*) 11 cm downstream of the DL showing the free electron population. The dashed lines show the tangential lines giving each temperature $T_{\text{e up trapped}}$ (8 eV), $T_{\text{e up tail}}$ (5 eV) and $T_{\text{e down}}$ (5 eV). The break energy of the EEDF depletion at 27 eV is defined as $\varepsilon_{\text{break}}$ and is close to the DL potential drop. (Reprinted with permission from Takahashi *et al* 2007, copyright American Institute of Physics.)

populations are present: the trapped electrons and the free electrons. Downstream of the DL, only one population of thermal electrons exists. These have recently been observed in the measured electron energy probability function (EEPF) using a RF compensated Langmuir probe (Takahashi *et al* 2007) and agree well with a particle in cell simulation (Meige and Boswell 2006). The results are shown in figure 20 for a pressure of 0.3 mTorr and the standard RF power and field configuration of the DL in the CHI KUNG device (Takahashi *et al* 2007). In the high potential plasma, upstream of the DL, the measured EEPF shows a very clear change in slope ($\varepsilon_{\text{break}}$) at energies corresponding to the double layer potential drop. Electrons with lower energy are Maxwellian with a temperature of 8 eV whereas those with higher energy have a temperature of 5 eV. The EEPF in the downstream plasma has a temperature of 5 eV. Over the range of pressures where the DL and accelerated ion beam is detected by a retarding field energy analyser (RFEA), the strength of the DL corresponds to the $\varepsilon_{\text{break}}$ in the EEPF as predicted by the particle in cell simulation (Meige and Boswell 2006). It is deduced that the downstream electrons come from upstream electrons that have sufficient energy to overcome the potential of the DL, and that only a single upstream plasma source is required to maintain this phenomenon. Recent radial measurements of the EEPF in the plasma cavity (Takahashi *et al* 2008) have shown even hotter electrons near the source tube wall (14 eV) associated with a skin effect. Radial EEPF measurements downstream of the DL have shown the importance and complexity of the diverging magnetic field on the final plasma equilibrium (Takahashi *et al* 2009).

5.4. Magnetic steering

The absence of grids or immersed electrodes in plasma thrusters limits the acceleration to a maximum of about 100 V since this is generally the highest plasma potential which can be obtained in the cavity. However, new control parameters, such as magnetic steering of the beam may be achieved. Steering has been recently demonstrated by using a transverse solenoid in addition to the two axial solenoids shown in figure 3(*b*) (Charles *et al* 2008c). Figure 21 shows the ion beam density profile and resulting steering angle measured as a function of the current in the transverse solenoid. An asymmetric exhaust is obtained which results from the perturbation in the applied magnetic field. For this range of current, the DL is maintained. These results suggest that full thruster magnetic steering capability could be obtained by adding a second transverse solenoid placed at 90° with respect to the first transverse solenoid. A transverse solenoid for each steering direction means additional electric power and weight to the plasma thruster but allows the supression of heavy gimbals currently used on satellites.

5.5. Alternative propellants

There is some interest in investigating alternative propellants and their associated chemistry. In principle the use of alternative reactive propellants may cause thruster, spacecraft and environmental contamination, may lead to a reduced spacecraft lifetime and are usually not an optimum choice in terms of thrust. However, potential applications include the use (thereby providing additional thrust) or transformation (thereby avoiding the high cost of toxic substances returned to Earth) of waste products in manned spacecraft, the use of propellant residuals (resulting from low tank pressures or from bi-propellant system tanks not emptying simultaneously) in chemically propelled spacecraft, or the use of propellants that are directly available in space (such as carbon dioxide

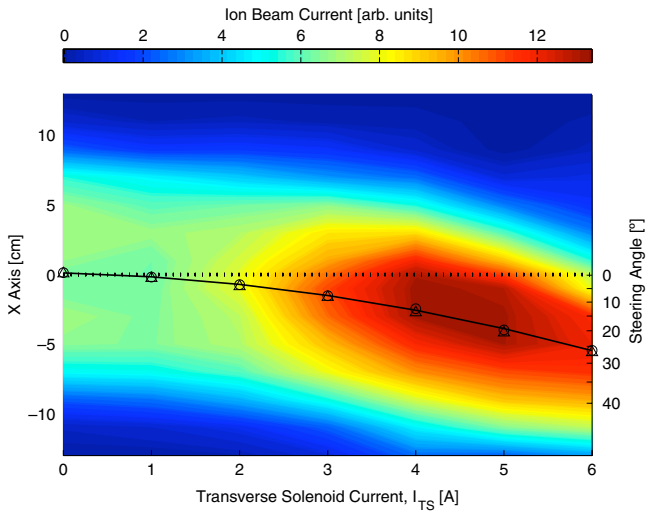

Figure 21. X-axial (radial) profile of the ion beam current measured in the CHI KUNG device as a function of I_{TS} for 250 W RF power and 0.3 mTorr pressure conditions (Charles *et al* 2008c). The triangles correspond to the midpoint between the FWHM x-axial positions of the ion beam current profiles and the circles show the half integral beam centre position, x_c. The solid line is the quadratic line of best fit through these circles. The right vertical axis shows the steering angle and is a non-linear scale, such that the positions of the triangles and circles also correspond to the steering angle axis. (Reprinted with permission from Charles *et al* 2008c, copyright American Institute of Physics.)

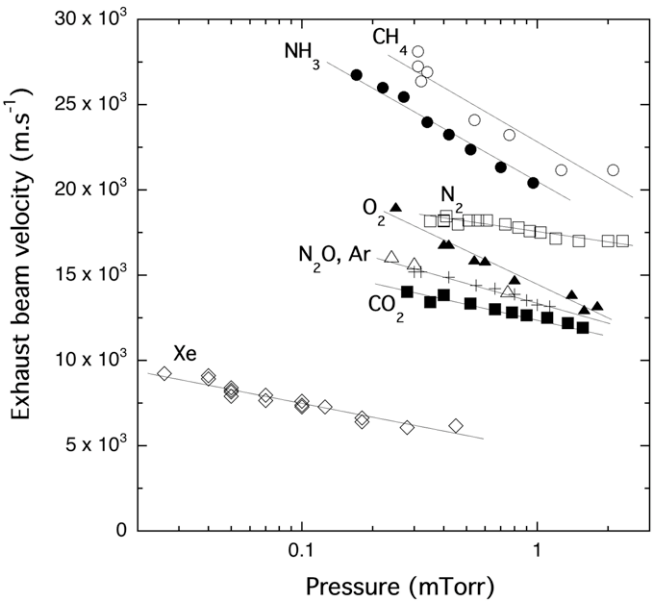

Figure 22. Exhaust velocity for various propellants measured in the CHI KUNG device (Charles 2008a, 2008b, Charles 2005a, 2005b, Charles *et al* 2006, Charles *et al* 2008b); Ar (crosses), N_2O (open triangles).

from the atmosphere of Mars or Venus). Figure 22 shows the exhaust velocity of the ion beam measured in the CHI KUNG device and in the HDLT (xenon) for a variety of common and alternative propellants. Details on the ion beam characteristics in methane, ammonia, nitrogen and nitrous oxide plasmas have been discussed (Charles *et al* 2008b) and are compared with the argon results (Charles 2005b) and to the xenon results (Charles *et al* 2006). The latter were obtained with a different pumping system attached to the CHI KUNG device (700 L s^{-1}). Although not shown in figure 22 for clarity, the results obtained using hydrogen (Charles 2004) lead to an exhaust velocity of about 70×10^3 m s^{-1} and the operating pressure range extends to higher pressures (a few millitorr). Figure 22 shows that the relative variation of the ion beam exhaust velocity versus operating pressure does not change much and on first approximation the velocity scales with the square of the ion mass for a constant geometry and magnetic field structure. Although the main external parameters do not strongly affect the position of the DL for a set geometry, the nature of the propellant does (Charles *et al* 2008b, 2009). For a particular propellant, the DL may be found inside (Charles 2007) or outside the source tube (Sutherland *et al* 2005b, Byhring *et al* 2008) depending on the geometry and magnetic field structure. Some of these plasmas may contain a small fraction of negative ions but essentially behave as electropositive gases (Charles 2002, Charles and Boswell 1995a). Data using oxygen and carbon dioxide plasmas have been presented (Charles *et al* 2009). The carbon dioxide results are attractive as this propellant is an important constituent in the atmosphere of planets such as Mars and Venus. Carbon dioxide is also a waste product of crewed missions and the International Space Station.

6. Electric propulsion based space missions

Hall thrusters have been profusely studied, developed and flown by the Russians under the appellation of stationary plasma thruster (SPT). Starting with the first successful satellite station-keeping mission launched in 1971, over 140 Hall thrusters have since been operated aboard satellites. The technology, developed into commercial thrusters by companies such as Fakel in Russia, is very successful. In 2003, ESA launched the SMART 1 mission to the Moon using a Hall thruster made by the French company SNECMA.

During the 1990s both Japan and the USA started operating gridded ion thrusters (e.g. XIOS thruster) on geosynchronous satellites, initially as 'proof of concept' missions followed by commercial flights (a total of about 100 to date). In 1998 NASA launched a dc electron bombardment discharge thruster on the DEEP SPACE 1 spacecraft. NASA's DAWN mission to Ceres and Vesta in the asteroid belt was launched in 2007, uses three ion gridded thrusters and the end of the primary mission is scheduled for 2015. In 2001 ESA launched the ARTEMIS mission with two technologies on board: the electron bombardment ion thruster assembly and the RF ion thruster assembly. ESA is also preparing the launch in 2013 the BepiColombo mission to Mercury. More recently (2003), JAXA (Japan Aerospace Exploration Agency) launched the MUSES-C/HAYABUSA spacecraft with microwave ion thrusters in an asteroid sample landing mission due to return samples to Earth in 2010.

In this review the discussion on power efficiency, mass utilization efficiency, total efficiency and detailed balance of the forces involved in the thrust has not gone into any depth. The power efficiency of flown ion gridded thrusters and flown

Hall thrusters varies with the thruster design and its operating parameters (which depend on mission requirements). The experimentally measured power efficiency is typically about 50% for a Hall thruster and ranges from 40% to 90% for an ion gridded thruster (Goebel and Katz 2008). For the case of a cylindrical electrode-less plasma source such as the helicon source, the interested reader can find information on this topic in a recent theoretical paper by Fruchtman (Fruchtman 2008). The thrust calculations derived in the present review are only rough estimates. Although momentum transfer in the case of a DL containing expanding plasma has also been discussed (Fruchtman 2006), a lot has yet to be unfolded. There are differing views on how these electrode-less plasma sources operate and to date there is no thrust versus input power data available in the literature for this type of thruster.

Inductive or wave coupled low pressure high density plasma sources such as the helicon source operate in a variety of coupling modes with large external parameter ranges and are attractive candidates for future electric propulsion missions. A considerable development effort is needed which has been initiated over the past decade worldwide. However, to date there have been no flown 'plasma' thrusters such as those defined in this review.

Acknowledgments

The author would like to thank PhD student Wes Cox for his help in the preparation of figures 15, 16 and 17 and PhD student Michael West for his help in the electric propulsion literature study. Many thanks to my Yamaha C5 grand piano for providing beautiful sounds during the preparation of this review and to the Tomaga River Mouth for providing beautiful waves during the endless summer 2008.

References

Aanesland A, Charles C, Boswell R W and Fredriksen 2003 *Plasma Sources Sci. Technol.* **12** 85
Aanesland A, Charles C, Boswell R W and Fredriksen 2004 *J. Phys. D: Appl. Phys.* **37** 1334
Aanesland A, Charles C, Boswell R W and Lieberman M A 2005 *Phys. Plasmas* **12** 103505
Aanesland A and Charles C 2006 *Phys. Scr.* T **122** 19
Aanesland A, Charles C, Lieberman M A and Boswell R W 2006a *Phys. Rev. Lett.* **97** 075003
Aanesland A, Lieberman M A, Charles C and Boswell R W 2006b *Phys. Plasmas* **13** 122101
Andrews J G and Allen J E 1971 *Proc. R. Soc. Lond.* A **320** 459
Arefiev A V and Breizman B N 2004 *Phys. Plasmas* **11** 2942
Arefiev A V and Breizman B N 2005 *Phys. Plasmas* **12** 043504
Baalrud S D, Hershkowitz N and Longmier B 2007 *Phys. Plasmas* **14** 042109
Bering E A, Chang-Diaz F R, Squire J P, Brukardt M, Glover T W, Bengston R D, Jacobson V T, McCaskill G E and Cassady L 2008 *Adv. Space Res.* **42** 192
Biloiu C, Sun X, Choueiri E, Doss F, Scime E E, Heard J, Spektor R and Ventura D 2005 *Plasma Sources Sci. Technol.* **14** 766
Biloiu I A, Scime E E and Biloiu C 2008 *Appl. Phys. Lett.* **92** 191502
Boswell R W 1970 *Phys. Lett.* A **33** 457
Boswell R W 1974 *PhD Thesis* Flinders University
Boswell R W 1984a *J. Plasm. Phys.* **31** 193
Boswell R W 1984b *Plasma Phys. Control. Fusion* **26** 1147
Boswell R W and Porteous R K 1987 *Appl. Phys. Lett.* **50** 1130
Boswell R W and Vender D 1995 *Plasma Sources Sci. Technol.* **4** 534
Boswell R W and Chen F F 1997 *IEEE Trans. Plasma Sci.* **25** 1229
Boswell R W, Perry A J and Emami M 1989 *J. Vac. Sci. Technol.* A **7** 3345
Boswell R, Porteous R, Prytz A, Bouchoule A and Ranson P 1982 *Phys. Lett.* A **91** 163
Boswell R W *et al* 2004 *Phys. Plasmas* **11** 5125
Boswell R W, Marsch E, Charles C 2006 *Astrophys. J.* **640** L199
Byhring H S, Charles C, Fredriksen A and Boswell R W 2008 *Phys. Plasmas* **15** 102113
Braithwaite N St J 2000 *Plasma Sources Sci. Technol.* **9** 517
Bramanti C, Izzo D, Samaraee T, Walker R and Fearn D 2009 *Acta Astronaut.* **64** 735
Brophy J R and Noca M 1998 *J. Propul. Power* **14** 700
Chakraborty Thakur S, Harvey Z, Biloiu I A, Hansen A, Hardin R A, Przybysz and Scime E E 2009 *Phys. Rev. Lett.* **102** 035004
Chang-Diaz F F 2000 *Sci. Am.* **283** 90
Charles C 1993 *J. Vac. Sci. Technol.* A **11** 157
Charles C 2002 *J. Vac. Sci. Technol.* A **20** 1275
Charles C 2003 *J. Phys. D: Appl. Phys.* **36** 2076
Charles C 2004 *Appl. Phys. Lett.* **84** 332
Charles C 2005a *Phys. Plasmas* **12** 044508
Charles C 2005b *IEEE Trans. Plasma Sci.* **33** 336
Charles C 2007 *Plasma Sources Sci. Technol.* **16** R1–25
Charles C and Boswell R W 1995a *J. Vac. Sci. Technol.* A **13** 2067
Charles C and Boswell R W 1995b *J. Appl. Phys* **78** 766
Charles C and Boswell R W 1998 *J. Appl. Phys.* **84** 350
Charles C and Boswell R W 2002 *Australian Patent Application Number 2003232523 (PCT/AU03/00763)* (June 19, 2002)
Charles C and Boswell R W 2003 *Appl. Phys. Lett.* **82** 1356
Charles C and Boswell R W 2004a *Phys. Plasmas* **11** 3808
Charles C and Boswell R W 2004b *Phys. Plasmas* **11** 1706
Charles C and Boswell R W 2007 *Appl. Phys. Lett.* **91** 201505
Charles C and Boswell R W 2008 *IEEE Trans. Plasma Sci.* **36** 2141
Charles C, Boswell R W, Bouchoule A, Laure C and Ranson P 1991 *J. Vac. Sci. Technol.* A **9** 661
Charles C, Boswell R W and Porteous R K 1992 *J. Vac. Sci. Technol.* A **10** 398
Charles C, Degeling A, Sheridan T, Harris, Lieberman M and Boswell R 2000 *Phys. Plasmas* **7** 5232
Charles C, Boswell R W and Lieberman M A 2003 *Phys. Plasmas* **10** 891
Charles C, Boswell R W and Lieberman M A 2006 *Appl. Phys. Lett.* **89** 261503
Charles C *et al* 2008a *IEEE Trans. Plasma Sci.* **36** 1196
Charles C, Boswell R W, Laine R and MacLellan P 2008b *J. Phys. D: Appl. Phys.* **41** 175213
Charles C, Boswell R W, Cox W, Laine R and MacLellan P 2008c *Appl. Phys. Lett.* **93** 201501
Charles C, Boswell R W and Hawkins R 2009 **97** in preparation
Chen F F 2008 *IEEE Trans. Plasma Sci.* **36** 2095
Chen F F and Boswell R W 1997 *IEEE Trans. Plasma Sci.* **25** 1245
Chi K-K, Sheridan T E and Boswell R W 1999 *Plasma Sources Sci. Technol.* **8** 421
Choueiri E Y 2001 *Phys. Plasmas* **8** 1411
Choueiri E Y 2004 *J. Propul. Power* **20** 193
Cohen S A, Siefert N S, Stange S, Boivin R F, Scime E E, Levinton F M 2003 *Phys. Plasmas* **10** 2593
Cohen S A, Sun X, Ferraro N M, Scime E E, Miah M, Stange S, Siefert N and Boivin R F 2006 *IEEE Trans. Plasma Sci.* **34** 792
Corr C W, Zanger J, Boswell R W and Charles C 2007 *Appl. Phys. Lett.* **91** 241501
Corr C S and Boswell R W 2007 *Phys. Plasmas* **14** 122503
Corr C W, Boswell R W, Charles C and Zanger J 2008 *Appl. Phys. Lett.* **92** 221508

Cox W, Charles C, Boswell R and Hawkins R 2008a *Appl. Phys. Lett.* **93** 071505

Cox W, Hawkins R, Charles C and Boswell R 2008b *IEEE Trans. Plasma Sci.* **36** 1386

Degeling A W, Jung C O, Boswell R W and Ellingboe A R 1996 *Phys. Plasmas* **3** 2788

Degeling A W 1999 *PhD Thesis* Australian National University

Deline C A, Bengston R D, Breizman B N, Tushentsov M R, Jones J E, Chavers D G, Dobson C C and Schuettpelz B M 2009 *Phys. Plasmas* **16** 033502

Denning C M, Wiebold M and Scharer J E 2008 *Phys. Plasmas* **15** 072115

Ergun R E, Andersson L, Main D, Su Y-J, Newman D L, Goldman M V, Carlson C W, Hull A J, McFadden J P and Mozer F S 2004 *J. Geophys. Res.* **109** A12220

Frisbee R H 2003 *J. Propul. Power* **19** 1129

Fruchtman A 2006 *Phys. Rev. Lett.* **96** 065002

Fruchtman A 2008 *IEEE Trans. Plasma Sci.* **36** 403

Fruchtman A and Cohen-Zur A 2006 *Appl. Phys. Lett.* **89** 111501

Gesto F N, Blackwell B D, Charles C and Boswell R W 2006 *J. Propul. Power* **22** 24

Gesto F N, Charles C and Boswell R W 2008 *IEEE Trans. Plasma Sci.* **36** 1194

Goebel D M 2008 *IEEE Trans. Plasma Sci.* **36** 2111

Goebel D M and Katz I 2008 *Fundamentals of Electric Propulsion* (Hoboken, USA: Wiley)

Gold H, Rulis R J, Maruna F A and Hawersaat W H 1964 *Description and operation of spacecraft in SERT I ion thrustor flight test, National Aeronautics and Space Administration, Washington, DC* NASA TM X-52050

Hairapetian G and Stenzel R L 1991 *Phys. Fluids* B **3** 899

Hass J M and Gallimore A D 2001 *Phys. Plasmas* **8** 652

Hershkowitz N 1985 *Space Sci. Rev.* **41** 351

Hershkowitz N 2005 *Phys. Plasmas* **12** 055502

Hippler R, Kredl J and Vartolomei V 2009 *Vacuum* **83** 732

Hooper E B 1993 *J. Propul. Power* **9** 757

Hussein M A and Emmert G A 1990 *J. Vac. Sci. Technol.* A **8** 2913

Inutake M, Ando A, Hattori K, Tobari H, Makita T, Shibata M, Kasashima Y and Komagome T 2007 *Plasma Phys. Control. Fusion* **49** A121

Jahn R G 2006 Edition *Physics of Electric Propulsion* (New York: Dover)

Jahn R G and Choueiri E Y 2002 *Encyclopedia of Physical Science and Technology* 3rd edn vol 5 (New york: Academic)

Kaganovich I D, Rozhansky V A, Tsendin L D and Yu Veseloca I 1996 *Plasma Sources Sci. Technol.* **5** 743

Keese A M, Scime E E, Charles C, Meige A and Boswell R W 2005 *Phys. Plasmas* **12** 093502

Keidar M, Boyd I D and Beilis I I 2000 *IEEE Trans. Plasma Sci.* **28** 376

Keidar M, Gallimore A D, Raitses Y and Boyd I D 2004 *Appl. Phys. Lett.* **85** 2481

Lafleur T, Charles C and Boswell R W 2009 *Phys. Plasmas* **16** 044510

Lieberman M A and Lichtenberg A J 1994 *Principles of Plasma Discharges and Materials Processing* (New York: Wiley-Interscience)

Lieberman M A and Charles C 2006 *Phys. Rev. Lett.* **97** 045003

Lieberman M A, Charles C and Boswell R W 2006 *J. Phys. D: Appl. Phys.* **39** 3294

Man K F, Smith A C H and Harrison M F A 1993 *J. Phys. B: At. Mol. Opt. Phys.* **26** 1365

Manheimer W M 2000 *IEEE Trans. Plasma Sci.* **28** 359

Manheimer W M 2001 *IEEE Trans. Plasma Sci.* **29** 75

Martinez-Sanchez M and Pollard J E 1998 *J. Propul. Power* **14** 688

Meige A, Boswell R W, Charles C and Turner M M 2005a *Phys. Plasmas* **12** 052317

Meige A, Boswell R W, Charles C, Boeuf J-P, Hagelaar G and Turner M M 2005b *IEEE Trans. Plasma Sci.* **33** 334

Meige A and Boswell R W 2006 *Phys. Plasmas* **13** 092104

Okuno K, Koizumi T and Kaneko Y 1978 *Phys. Rev. Lett.* **40** 1708

Perry A J, Vender D and Boswell R W 1991 *J. Vac. Sci. Technol.* B **9** 310

Perry A J, Conway G, Boswell R W and Persing H 2002 *Phys. Plasmas* **9** 3171

Porteous R K and Boswell R W 1987 *J. Appl. Phys* **50** 1130

Plihon N, Corr C S and Chabert P 2005 *Appl. Phys. Lett.* **86** 091501

Pullins S H, Dressler R A, Torrents R and Gerlich D 2000 *Z. Phys. Chem.* **214** 1279

Raitses Y, Keidar M, Staack D and Fisch N J 2002 *J. Appl. Phys.* **92** 4906

Rudakov D L, Shats M G, Boswell R W, Charles C and Howard J 1999 *Rev. Sci. Instrum.* **70** 476

Sack C, Schamel H and Schmalz R 1986 *Phys. Fluids* **29** 1337

Scott Miller J, Pullins S H, Levandier D J, Chiu Y and Dressler R A 2002 *J. Appl. Phys.* **91** 984

Sheridan T E and Chi K-K 2000 *Phys. Lett.* A **271** 391

Singh N and Khazanov G 2003 *J. Geophys. Res.* **108** 8007

Smith H, Charles C, Boswell R W and Kuwahara 1997 *J. Appl. Phys.* **82** 561

Smith H, Charles C and Boswell R W 2003 *Phys. Plasmas* **10** 875

Strinic A I, Malovic G N, Petrovic Z Lj and Sadeghi N 2004 *Plasma Sources Sci. Technol.* **13** 333

Sun X, Keesee A M, Biloiu C, Scime E E, Meige A, Charles C and Boswell R W 2005 *Phys. Rev. Lett.* **95** 025004

Sutherland O, Ankiewicz A and Boswell R W 2005a *Phys. Plasmas* **12** 033103

Sutherland O, Charles C, Plihon N and Boswell R W 2005b *Phys. Rev. Lett.* **95** 205002

Taccogna F, Schneider R, Longo S and Capitelli M 2008 *Plasma Sources Sci. Technol.* **17** 024003

Takahashi K, Charles C, Boswell R W, Kaneko T and Hatakeyama R 2007 *Phys. Plasmas* **14** 114503

Takahashi K, Charles C, Boswell R W and Hatakeyama R 2008 *Phys. Plasmas* **15** 074505

Takahashi K and Fujiwara T 2009 *Appl. Phys. Lett.* **94** 061502

Takahashi K, Charles C, Boswell R W, Cox W and Hatakeyama R 2009 *Appl. Phys. Lett.* **94** 191503

Tanabe Y *et al* 1994 *Japan. J. Appl. Phys.* **33** 6684

Turner M J L 2009 *Rocket and Spacecraft Propulsion* (Chichester, UK: Springer Praxis Publishing Ltd)

Toki K, Shinohara S, Tanikawa T and Shamrai K P 2006 *Thin Solid Films* **506** 597

Virko Y V, Virko V F, Shamrai K P and Yakimenko A I 2007 *Prob. At. Sci. Technol.* **1** 136

Walker R, Bramanti C, Sutherland O, Boswell R W, Charles C, Fearn D, Gonzalez Del Amo J, Frigot P-E and Orlandi M 2006 *Proc. 42nd AIAA.ASME/SAE/ASEE Joint Propulsion Conf. (Sacramento, USA, July 2006)*

West M D, Charles C and Boswell R W 2008 *J. Propul. Power* **24** 134

West M D, Charles C and Boswell R W 2009 *Rev. Sci. Instrum.* **80** 053509

Yoon H J, Charles C and Boswell R W 2005 *J. Phys. D: Appl. Phys.* **38** 2825

Zhurin V V, Kaufman H R and Robinson R S 1999 *Plasma Sources Sci. Technol.* **8** R1–20